Hydrodynamic interactions in ion transport—Theory and simulation

Diddo Diddens ■ (i); Andreas Heuer (ii)



J. Chem. Phys. 158, 154112 (2023)

https://doi.org/10.1063/5.0147339





CrossMark



Chemical Physics Reviews

Special Topic: Molecular Approaches for Spin-based Technologies

Submit Today!





Hydrodynamic interactions in ion transport—Theory and simulation

Cite as: J. Chem. Phys. 158, 154112 (2023); doi: 10.1063/5.0147339

Submitted: 21 February 2023 · Accepted: 24 March 2023 ·

Published Online: 20 April 2023











AFFILIATIONS

- ¹ Helmholtz Institute Münster: Ionics in Energy Storage (IEK-12), Forschungszentrum Jülich GmbH, Corrensstraße 46, 48149 Münster, Germany
- Institut für physikalische Chemie, Westfälische Wilhelms-Universität Münster, Corrensstraße 28/30, 48149 Münster, Germany
- a)Author to whom correspondence should be addressed: d.diddens@fz-juelich.de
- b)Electronic mail: andheuer@uni-muenster.de

ABSTRACT

We present a hydrodynamic theory describing pair diffusion in systems with periodic boundary conditions, thereby generalizing earlier work on self-diffusion [B. Dünweg and K. Kremer, J. Chem. Phys. 99, 6983-6997 (1993) and I.-C. Yeh and G. Hummer, J. Phys. Chem. B 108, 15873-15879 (2004)]. Its predictions are compared with Molecular Dynamics simulations for a liquid carbonate electrolyte and two ionic liquids, for which we characterize the correlated motion between distinct ions. Overall, we observe good agreement between theory and simulation data, highlighting that hydrodynamic interactions universally dictate ion correlations. However, when summing over all ion pairs in the system to obtain the cross-contributions to the total cationic or anionic conductivity, the hydrodynamic interactions between ions with like and unlike charges largely cancel. Consequently, significant conductivity contributions only arise from deviations from a hydrodynamic flow field of an ideal fluid, which is from the local electrolyte structure as well as the relaxation processes in the subdiffusive regime. In the case of ionic liquids, the momentum-conservation constraint additionally is vital, which we study by employing different ionic masses in the simulations. Our formalism will likely also be helpful to estimate finite-size effects of the conductivity or of Maxwell-Stefan diffusivities in simulations.

© 2023 Author(s). All article content, except where otherwise noted, is licensed under a Creative Commons Attribution (CC BY) license (http://creativecommons.org/licenses/by/4.0/). https://doi.org/10.1063/5.0147339

I. INTRODUCTION

Due to the increasing demand for renewable energies, substantial efforts are currently being made to develop novel electrolytes for energy storage devices. ^{1,2} For contemporary lithium-ion batteries, liquid carbonate-based electrolytes remain important as well-established materials that can deliberately be fine-tuned via additives. 1,2 On the other hand, ionic liquids (ILs) are a more novel class of materials that are promising for, e.g., supercapacitors, as they are solely composed of cations and anions and hence have high charge densities.3

With respect to the application of these materials as electrolytes, the ionic conductivity

$$\sigma = \sigma_+ + \sigma_- \,, \tag{1}$$

containing contributions from both cations (σ_+) and anions (σ_-) , as well as the transference numbers

$$t_{\pm} = \frac{\sigma_{\pm}}{\sigma_{+} + \sigma_{-}},\tag{2}$$

of cations and anions, respectively, are key design parameters. Most generally, experimental measurements of σ_{\pm} and t_{\pm} can be achieved by electrophoretic nuclear magnetic resonance (eNMR)⁵⁻¹⁰ or combined techniques with additional assumptions. 11-13 For polymer electrolytes, the well-established Bruce-Vincent method is another viable option.¹

On the other hand, σ_{\pm} and t_{\pm} can readily be calculated from Molecular Dynamics (MD) simulations, given sufficient sampling. In particular, the linear-response conductivity can be extracted from equilibrium MD simulations as follows:1

$$\sigma = \lim_{\Delta t \to \infty} \frac{e^2}{6V \, \Delta t \, k_{\rm B} T} \sum_{i=1}^{N} \sum_{j=1}^{N} z_i z_j \, \langle \Delta \mathbf{r}_i \, \Delta \mathbf{r}_j \rangle. \tag{3}$$

Here, z_i and z_j are the valencies of ions i and j contained in volume V, e is the elementary charge, k_BT is the thermal energy, and $\Delta \mathbf{r}_i$ and $\Delta \mathbf{r}_i$ are the displacement vectors of ions *i* and *j* during lag time Δt . If well-defined and long-lived ion pairs of cations and anions existed, it is obvious that the net conductivity would be reduced by their

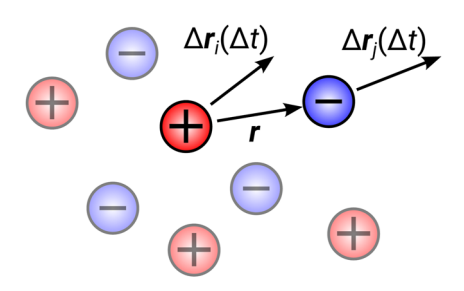


FIG. 1. Schematic illustration of the distance and displacement vectors used in this study. Motional correlations of two different ions are expressed by the average scalar product between their displacement vectors $\Delta \mathbf{r}_i$ and $\Delta \mathbf{r}_j$ in dependence on their initial distance r.

presence, as such pairs would contribute to the *mass* transport (and thus to the diffusion coefficients D_{\pm}), but not to the *charge* transport measured by σ . Such a reduction is indeed seen from Eq. (3) for cation–anion pairs that move cooperatively into a certain direction due to the fact that $\langle \Delta {\bf r}_i \ \Delta {\bf r}_j \rangle > 0$ in this case, which diminishes σ (see the sketch in Fig. 1). However, the picture of distinct ion pairs is generally an oversimplification: First, larger ion clusters might form in an electrolyte, ^{18–22} and second, ion pairs or clusters are temporal in nature, i.e., they continuously disintegrate and reform. ^{18,19,22,23} Nonetheless, distinct ions move correlated (or anticorrelated) in any non-ideal electrolyte with finite concentration, which consequently affects the value of σ .

To study these ionic correlations in an electrolyte with monovalent ions $(z_{\pm}=\pm 1)$ in more detail, we define

$$\sigma_{++} = \lim_{\Delta t \to \infty} \frac{e^2}{6V \, \Delta t \, k_B T} \sum_{i=1}^{N_+} \sum_{j=1}^{N_+} \langle \Delta \mathbf{r}_i \, \Delta \mathbf{r}_j \rangle, \tag{4a}$$

$$\sigma_{+-} = \lim_{\Delta t \to \infty} \frac{-e^2}{6V \, \Delta t \, k_{\rm B} T} \sum_{i=1}^{N_+} \sum_{j=1}^{N_-} \left\langle \Delta \mathbf{r}_i \, \Delta \mathbf{r}_j \right\rangle,\tag{4b}$$

$$\sigma_{--} = \lim_{\Delta t \to \infty} \frac{e^2}{6V \, \Delta t \, k_{\rm B} T} \sum_{i=1}^{N_{-}} \sum_{j=1}^{N_{-}} \left\langle \Delta \mathbf{r}_i \, \Delta \mathbf{r}_j \right\rangle, \tag{4c}$$

with N_+ and N_- being the numbers of cations and anions, respectively, and $N_+ + N_- = N$ as well as $N_+ = N_-$ due to electroneutrality. In this way, Eq. (3) may be decomposed into individual contributions arising from the collective motion of cations and cations, anions and anions, as well as cations and anions^{12,13} (the former two additionally containing the self-diffusion of the respective ion species),

$$\sigma = \sigma_{++} + 2\sigma_{+-} + \sigma_{--}. \tag{5}$$

With the additional definitions

$$\sigma_{+} = \sigma_{++} + \sigma_{+-}, \tag{6a}$$

and

$$\sigma_{-} = \sigma_{+-} + \sigma_{--}. \tag{6b}$$

Equation (1) is recovered.

In addition, these general definitions valid for any electrolyte, ILs by definition lack a neutral solvent, such that the system only consists of cations and anions. This has the important consequence that in periodic systems, momentum conservation affects the charge

transport because there are no solvent molecules that can exchange momentum with the ions. Although this was already shown in early analytical calculations on molten salts, ^{24,25} Kashyap *et al.* more recently confirmed the same mechanism for ILs via both analytical calculations and MD simulations. ²⁶ A similar impact of momentum conservation on the ionic cross-correlations has been observed for other quasi-binary mixtures. ^{9,27} In particular, because the center of mass of the system is at rest,

$$m_{+}\sum_{i=1}^{N_{+}} \Delta \mathbf{r}_{i} + m_{-}\sum_{i=1}^{N_{-}} \Delta \mathbf{r}_{i} = 0,$$
 (7)

where m_{\pm} are the masses of cations and anions, respectively. Multiplying this expression by $\sum_{j=1}^{N_{+}} \Delta \mathbf{r}_{j}$ (or $\sum_{j=1}^{N_{-}} \Delta \mathbf{r}_{j}$) and taking the average yields

$$m_{+} \sum_{i=1}^{N_{+}} \sum_{j=1}^{N_{+}} \langle \Delta \mathbf{r}_{i} \Delta \mathbf{r}_{j} \rangle + m_{-} \sum_{i=1}^{N_{-}} \sum_{j=1}^{N_{+}} \langle \Delta \mathbf{r}_{i} \Delta \mathbf{r}_{j} \rangle = 0.$$
 (8)

Inserting all possible combinations of the expressions in Eq. (4) into Eq. (8), using the short-hand notations from Eqs. (5) and (6), accounting for the valencies z_i and z_j in Eq. (3) and rearranging we arrive at

$$\frac{\sigma_{++}}{\sigma_{+-}} = \frac{m_-}{m_+},\tag{9a}$$

$$\frac{\sigma_{--}}{\sigma_{+-}} = \frac{m_+}{m_-},$$
 (9b)

$$\frac{\sigma_{++}}{\sigma_{--}} = \frac{m_{-}^2}{m_{+}^2},\tag{9c}$$

$$\frac{\sigma_+}{\sigma} = \frac{m_-}{m_-}.$$
 (9d)

A particularly interesting implication pointed out by Kashyap *et al.*²⁶ is that $\sigma_{+-} > 0$, which mathematically arises from the fact that $\sigma_{++} > 0$ and $\sigma_{--} > 0$ due to the dominant self-diffusion terms. This is in clear contrast to what is typically found for electrolytes including a solvent, in which the cooperative motion of cations and anions reduces σ , that is $\sigma_{+-} < 0$. Because in an IL, the motion of any ion has to be compensated by the motion of all other ions, on a global scale, cations and anions (but also ions with equal charges) move anticorrelated, i.e., in opposite directions, ²⁶ such that $\langle \Delta \mathbf{r}_i \Delta \mathbf{r}_j \rangle_{+-} < 0$, resulting in $\sigma_{+-} > 0$ due to $z_i z_j = -1$.

Nonetheless, one would intuitively expect that locally, neighboring ions with opposite charges move correlated. Via a distance-resolved analysis of the σ_{XY} in Eq. (5) (with X and Y denoting the two ion species "+" and "–"), Tu $et~al.^{28}$ showed that in ILs, neighboring ions indeed move correlated, whereas the dominating anticorrelated motion emerges only for larger interionic separations. Interestingly, also equally charged ions displayed locally correlated dynamics. ²⁸ Furthermore, Tu et~al. demonstrated that qualitatively, the same features are also found for conventional aqueous electrolytes, ^{29,30} although $\sigma_{+-} < 0$ as naively expected. In a recent paper, we could also confirm the correlated motion between lithium ions and their anionic solvation shell in IL/Li-salt mixtures with varying salt fractions. ²²

In the present contribution, we aim to understand the distance dependence of the σ_{XY} in more detail. To this end, we derive an

analytical framework to capture the distance dependence of σ_{XY} based on a hydrodynamic theory that has originally been developed to calculate finite-size effects of the self-diffusion in periodic systems. ^{31–35} These theoretical predictions are then compared with the MD simulation data for a liquid carbonate electrolyte (CE) and an IL. The remainder of this paper is organized as follows: In Sec. II, we describe the technical aspects of the MD simulations, whereas in Sec. III, we develop our hydrodynamic framework for pair diffusion in periodic systems and compare it with the distance-dependent ion correlations extracted from the MD data. We then study the time dependence of these ionic correlations in light of our theory in Sec. IV. Finally, in Sec. V, we conclude and give an outlook on how our framework could contribute to related topics.

II. SIMULATION DETAILS

The MD simulations have been performed with the simulation code Lucretius developed at the University of Utah using the APPLE & P polarizable force field. For the CE, we reused MD trajectories from an earlier study,17 which is an equimolar mixture of ethylene carbonate (EC) and dimethyl carbonate (DMC) with 1 mol/l lithium bis(trifluoromethane)sulfonimide (LiTFSI). In addition, we simulated two ILs, namely 1-ethyl-3-methylimidazolium TFSI ([EMIm][TFSI]) and EMIm tetrafluoroborate ([EMIm][BF₄]). For the sake of clarity, only the data for [EMIm][TFSI] are shown in the main text, whereas the corresponding data for [EMIm][BF₄] is given in the Appendix. The ILs contained 256 ion pairs inside a cubic simulation box. In addition to the systems with standard masses, comparative simulations with artificially modified masses have been performed to assess the impact of momentum conservation on transport properties. For this purpose, the cation masses were scaled by a factor of $1/\sqrt{2}$, whereas the anion masses have been increased by a factor $\sqrt{2}$.

The systems were equilibrated for 5 ns in the NpT ensemble, followed by subsequent production runs of 100 ns in the NVT ensemble at 298 K, resulting in box lengths of 47.7589 and 40.5430 Å for [EMIm][TFSI] and [EMIm][BF₄], respectively. Both the temperature and the pressure of the system were maintained by a Nosé-Hoover chain thermostat (coupling frequency 0.01 fs⁻¹) and barostat (coupling frequency 0.0005 fs⁻¹),³⁸ whereas periodic boundary conditions were applied in all dimensions. Electrostatic interactions have been treated by the Ewald summation technique with a cutoff radius of 12 Å, an inverse Gaussian charge width of 0.23 Å^{-1} , and $7 \times 7 \times 7$ vectors for the reciprocal space. Lennard-Jones interactions have been truncated at 12 Å, beyond which a continuum-model dispersion correction was applied. All bonds were constrained by the SHAKE algorithm. ^{39,40} A multiple time-step integration scheme 41,42 was used to integrate the equations of motion, where a time step of 0.5 fs has been used for bonds and angles. For torsions and non-bonded interactions up to a distance of 7 Å, a time step of 1.5 fs was used, and finally, for non-bonded interactions between atoms separated more than 7 Å and the reciprocal part of the Ewald summation, a time step of 3 fs was used. The induced dipoles were determined iteratively where the corresponding dipole-dipole interactions were scaled to zero by a tapering function between 11 and 12 Å. The pressure tensor was dumped every 0.9 ps to calculate the viscosity (Sec. IV A and Appendix C).

The CE from the previous study¹⁷ was simulated in an NpT ensemble, for which the unwrapping of the ions' coordinates from the primary simulation box into real space can be problematic.^{43,44} In the present work, we observed a similar effect for pair diffusion. Therefore, the algorithm described in Ref. 43 was employed.

III. HYDRODYNAMIC THEORY

A. Distance dependence of ionic correlations

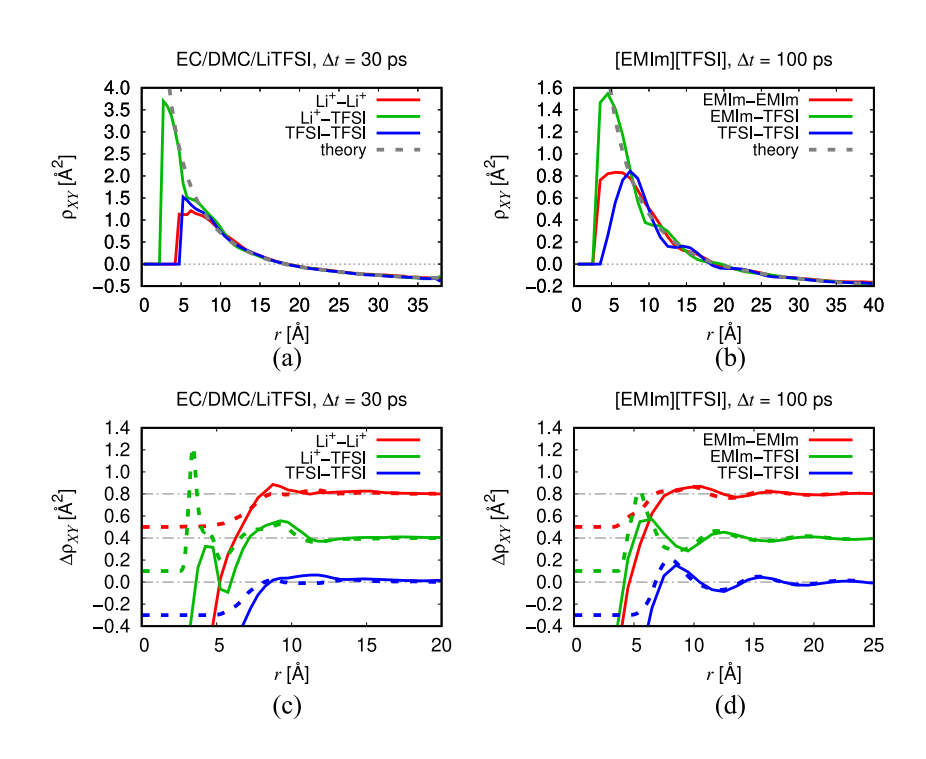
We start by characterizing the distance dependence of the ionic correlations $\langle \Delta \mathbf{r}_i \ \Delta \mathbf{r}_j \rangle$ in Eqs. (3) and (4). To this end, we define the dynamical correlation between two distinct ions as a function of their initial separation r:

$$\rho_{XY}(r) = \langle \Delta \mathbf{r}_i \, \Delta \mathbf{r}_j | r_{ij}(0) = r \rangle_{XY}, \tag{10}$$

where X and Y denote the ion species as above. The index at the $\langle \ldots \rangle_{XY}$ bracket indicates that the average is taken for a given pair type. In addition, only ion pairs with a given initial separation $r_{ij}(0) = r$ are averaged, as indicated by the conditional expression in Eq. (10).

The individual ρ_{XY} are shown in Fig. 2(a) for the CE with $\Delta t = 30$ ps and Fig. 2(b) for the IL with $\Delta t = 100$ ps. Here, the Δt values have been chosen such that the dynamics is still subdiffusive to avoid that the distance between the ions changes too much during Δt , which would blur the ρ_{XY} -curves in Fig. 2. However, the behavior for larger Δt up to a few nanoseconds is qualitatively the same, which we analyze below in Sec. IV. From Fig. 2, we observe that the curves of all pair types display a peak with $\rho_{XY} > 0$ at short initial separations (i.e., at about 5-10 Å), demonstrating that locally, all ion pairs move correlated. Similar observations have been made previously by Tu et al. 28,29 The short-range peak for the cation-anion correlation is larger than the respective peaks of ρ_{++} and ρ_{--} and shifted to shorter distances. This observation can be rationalized by the local ordering, i.e., the nearest-neighbor shell of a cation is essentially composed of anions and vice versa, 17,23,45,46 resulting in peak positions of ρ_{+-} shifted to shorter r and showing a larger magnitude. In the case of the IL, all ρ_{XY} show a decay superimposed with minor oscillations at intermediate distances, presumably related to its long-ranged ordering. ^{23,45,46} At large separations, all ρ_{yy} become increasingly negative for both systems, although the curves vary only slowly with r, demonstrating that the ions move anticorrelated, which is in agreement with the findings of Tu et al.2

In previous studies, 26,28 the anticorrelated motion has (at least partly) been attributed to the momentum conservation constraint. That is because locally all ion types move correlated, momentum conservation can only be realized by a compensating counterflux of ions at larger length scales. However, from Fig. 2(a), we observe anticorrelated motion at large r also for the CE, in line with previous results for an aqueous electrolyte. In fact, the qualitative shape of all ρ_{XY} in Fig. 2 is remarkably similar for larger r, pointing toward a universal feature. Empirically, we find that the decay of ρ_{XY} scales as 1/r, which is indicative of hydrodynamic interactions. As the 1/r-scaling is theoretically expected even when neglecting inertial forces, t^{47} the incompressibility of the medium must play an important role, too. Indeed, early analytical descriptions of the ionic conductivity assumed the existence of a hydrodynamic flow field



2. and Distance-(a) (b): dependent correlation $\rho_{XY}(r)$ $= \langle \Delta \mathbf{r}_i \, \Delta \mathbf{r}_i | r_{ij}(0) = r \rangle_{XY}$ ion pair types X and Y in dependence of their initial distance r. (c) and (d): Deviations of the simulation data from the hydrodynamic fit $(\Delta \rho_{XY} = \rho_{XY} - \rho_{PBC})$ solid curves) in comparison with the scaled and shifted RDFs (dashed curves). Several curves in (c) and (d) have been shifted for better visibility. The uncertainties are in the range of the line thickness.

around a given central ion. ^{48–51} Furthermore, the hydrodynamic picture is also in line with our recent findings for IL/Li-salt blends, where we observed that a given anion still moves cooperatively with a nearby lithium ion even after disengaging from its coordination shell.²² In the following, we therefore provide a theoretical basis for the observations in Figs. 2(a) and 2(b).

B. Pair diffusion in periodic systems

1. Two derivations of the pair diffusion tensor

Starting from Eq. (3), we define the diffusion tensor with the elements, 32,35

$$D_{ij}^{\beta\gamma} = \lim_{\Delta t \to \infty} \frac{\langle \Delta r_i^{\beta} \, \Delta r_j^{\gamma} \rangle}{6\Delta t},\tag{11}$$

describing the pair diffusion of ions i and j, where β and γ denote the spatial compounds of $\Delta \mathbf{r}_i$ and $\Delta \mathbf{r}_j$, respectively. For i=j in isotropic systems, the trace of this expression reduces to the well-known Einstein relation:

$$D_i = \lim_{\Delta t \to \infty} \frac{\langle \Delta \mathbf{r}_i^2 \rangle}{6\Delta t}.$$
 (12)

Rather than focusing on explicit pairs of ions, one may define the diffusion tensor as a function of the interionic separation $\mathbf{r} = \mathbf{r}_j - \mathbf{r}_i$ for $i \neq j$, ^{32,35} similar in spirit to Eq. (10):

$$\mathbf{D}_{ij} = \mathbf{D}(\mathbf{r}_j - \mathbf{r}_i). \tag{13}$$

For an infinite system, the diffusion tensor is given to first order (i.e., within the approximation of point particles valid for large r) by the so-called Oseen tensor,⁴⁷

$$\mathbf{D}_{\infty}(\mathbf{r}) = \frac{k_{\mathrm{B}}T}{8\pi\eta\mathbf{r}} (1 + \hat{\mathbf{r}}\hat{\mathbf{r}}), \tag{14}$$

that describes the hydrodynamic interactions in a fluid with viscosity η . For a cubic periodic system with box length L, analogous expressions were derived, ^{32,34} which we sketch in the following.

a. Green-Kubo relation. Dünweg 32 expressed Eq. (13) via the Green-Kubo relation

$$\mathbf{D}_{ij}(\mathbf{r}) = \int_0^\infty dt \, \langle \mathbf{u}(0,0)\mathbf{u}(\mathbf{r},t) \rangle, \tag{15}$$

where $\mathbf{u}(\mathbf{r},t)$ is the flow field in a continuous representation. From a set of discrete particles with positions $\{\mathbf{r}_i\}$, the latter can be obtained via $\mathbf{u}(\mathbf{r},t) = (V/N)\sum_{i=1}^N \mathbf{v}_i \delta(\mathbf{r} - \mathbf{r}_i)$, with $\{\mathbf{v}_i\}$ being the particles' velocities. Due to periodicity, $\mathbf{u}(\mathbf{r},t)$ can be expressed by its Fourier modes, i.e.,

$$\mathbf{u}(\mathbf{r},t) = \sum_{\mathbf{k}} \tilde{\mathbf{u}}_{\mathbf{k}}(t) \exp(i\mathbf{k} \cdot \mathbf{r})$$

$$\tilde{\mathbf{u}}_{\mathbf{k}}(t) = \frac{1}{N} \sum_{i=1}^{N} \mathbf{v}_{i}(t) \exp(-i\mathbf{k} \cdot \mathbf{r}_{i}),$$
(16)

where $\mathbf{k} = 2\pi \mathbf{n}/L$ is a reciprocal lattice vector with $\mathbf{n} = (n_x n_y n_z)^T$ and n_x , n_y , and $n_z \in \mathbb{Z}$. The diffusion tensor in the case of uncorrelated modes then reads³²

$$\mathbf{D}_{\mathrm{PBC}}(\mathbf{r}) = \sum_{\mathbf{k} \neq \mathbf{0}} (1 - \hat{\mathbf{k}}\hat{\mathbf{k}}) \exp(i\mathbf{k} \cdot \mathbf{r}) \int_0^\infty dt \, \langle \tilde{\mathbf{u}}_{\mathbf{k}}(0)\tilde{\mathbf{u}}_{\mathbf{k}}(t) \rangle, \quad (17)$$

[note that $(1 - \hat{\mathbf{k}}\hat{\mathbf{k}})$ projects on the transversal modes relevant for an incompressible system and "PBC" stands for "periodic boundary conditions"]. The zeroth mode is excluded, as it describes the net motion of the entire system.^{32,34} Dünweg evaluated the Green-Kubo integral on the right-hand side of Eq. (17) via the Mori-Zwanzig formalism, yielding^{32,35}

$$\int_0^\infty dt \, \langle \tilde{\mathbf{u}}_{\mathbf{k}}(0) \tilde{\mathbf{u}}_{\mathbf{k}}(t) \rangle = \frac{(k_{\rm B}T)^2}{k^2 V^2 \int_0^\infty dt \, \langle P_{\beta \gamma}(0) P_{\beta \gamma}(t) \rangle},\tag{18}$$

where the

$$P_{\beta \gamma}(t) = \frac{1}{V} \sum_{i=1}^{M} m_i v_{i\beta}(t) v_{i\gamma}(t) + F_{i\beta}(t) r_{i\gamma}(t), \qquad (19)$$

are the off-diagonal elements of the pressure tensor $(\beta \neq \gamma)$, m_i is the mass, $v_{i\beta}$ is the velocity, $F_{i\beta}$ is the force, and $r_{i\beta}$ is the position of particle i in the β -direction, respectively. Note that M in Eq. (19) denotes the total number of particles/atoms as opposed to the number of ions N and hence may also include a solvent. The integral in the denominator of Eq. (18) is nothing else than the Green-Kubo relation for the viscosity, 34,52

$$\eta = \frac{V}{k_{\rm B}T} \int_0^\infty dt \langle P_{\beta \gamma}(0) P_{\beta \gamma}(t) \rangle, \tag{20}$$

such that Eq. (17) becomes

$$\mathbf{D}_{PBC}(\mathbf{r}) = \frac{k_{\rm B}T}{V\eta} \sum_{\mathbf{k} \neq \mathbf{0}} \frac{(1 - \hat{\mathbf{k}}\hat{\mathbf{k}}) \exp{(i\mathbf{k} \cdot \mathbf{r})}}{k^2}.$$
 (21)

b. Stokes equation. An alternative route to Eq. (21) is via the Stokes equation,

$$\eta \nabla^2 \mathbf{u}(\mathbf{r}) = \nabla p(\mathbf{r}) - \left(\delta(\mathbf{r}) - \frac{1}{V}\right) \mathbf{F},$$
(22)

as shown by Yeh and Hummer,³⁴ where p is the pressure and \mathbf{F} is a perturbative force acting on a point-like particle. The term 1/V ensures that the net force acting on the periodic cell is zero, leading to the exclusion of the zeroth mode (see above). For an incompressible fluid with $\nabla \mathbf{u} = 0$, the divergence of Eq. (22) simplifies to

$$\nabla^2 p(\mathbf{r}) = \mathbf{F} \cdot \nabla \left(\delta(\mathbf{r}) - \frac{1}{V} \right). \tag{23}$$

Equations (22) and (23) can be transformed into the Fourier space via Eq. (16) and $p(\mathbf{r}, t) = \sum_{\mathbf{k}} \tilde{p}_{\mathbf{k}}(t) \exp(i\mathbf{k} \cdot \mathbf{r})$, giving

$$-\eta k^2 \tilde{\mathbf{u}}_{\mathbf{k}} = i\mathbf{k}\tilde{p}_{\mathbf{k}} - (1 + \delta_{\mathbf{k}})\mathbf{F},\tag{24}$$

and

$$-k^2 \tilde{p}_{\mathbf{k}} = i(1 - \delta_{\mathbf{k}}) \mathbf{k} \cdot \mathbf{F}. \tag{25}$$

Eliminating $\tilde{p}_{\mathbf{k}}$, rearranging, summing over all modes and using $\mathbf{u} = (k_{\rm B}T)^{-1} \mathbf{D}_{\rm PBC} \cdot \mathbf{F}$ results in Eq. (21) as well.

2. Trace of the diffusion tensor

Assuming that the relative orientation of the displacement vectors $\Delta \mathbf{r}_i$ and $\Delta \mathbf{r}_j$ is statistically independent from that of \mathbf{r} , we may take the trace of the tensors in Eqs. (14) and (21) to yield

$$D_{\infty}(r) = \frac{k_{\rm B}T}{6\pi\eta r},\tag{26}$$

for infinite systems and

$$D_{\text{PBC}}(r) = \frac{k_{\text{B}}T}{6\pi\eta} \frac{1}{V} \sum_{\mathbf{k}=\mathbf{0}} \frac{4\pi}{k^2} \exp\left(i\mathbf{k} \cdot \mathbf{r}\right), \tag{27}$$

for periodic systems. Thus, for an infinite system, we recover the Oseen-like decay³²⁻³⁴ proportional to 1/r, whereas in a periodic system, a more intricate distance dependence is found.

3. Ewald summation

Due to the fact that the summation in Eq. (27) is ill-convergent, one usually applies the Ewald summation technique, $^{33-35,53}$ in which an additional convergence factor $\exp(-k^2/(4\alpha^2))$ and a short-ranged compensating real-space summation is introduced to the summands in Eq. (27), 34,53 resulting in

$$D_{\text{PBC}}(r) = \frac{k_{\text{B}}T}{6\pi\eta} \left[\frac{1}{V} \sum_{\mathbf{k}\neq\mathbf{0}} \frac{4\pi}{k^2} \exp\left(i\mathbf{k} \cdot \mathbf{r}\right) \exp\left(-\frac{k^2}{4\alpha^2}\right) + \sum_{\mathbf{n}} \frac{\text{erfc}(\alpha|\mathbf{r} + \mathbf{n}L|)}{|\mathbf{r} + \mathbf{n}L|} - \frac{\pi}{V\alpha^2} \right].$$
(28)

The finite-size correction $\Delta D_{\rm FSC}(r) = D_{\rm PBC}(r) - D_{\infty}(r)$ for the comparison between periodic and the infinite systems can then be written as

$$\Delta D_{\text{FSC}}(r) = D_{\text{PBC}} - D_{\infty} = \frac{k_{\text{B}}T}{6\pi\eta} \left[\frac{1}{V} \sum_{\mathbf{k} \neq \mathbf{0}} \frac{4\pi}{k^2} \exp\left(i\mathbf{k} \cdot \mathbf{r}\right) \exp\left(-\frac{k^2}{4\alpha^2}\right) + \sum_{\mathbf{n} \neq \mathbf{0}} \frac{\operatorname{erfc}(\alpha|\mathbf{r} + \mathbf{n}L|)}{|\mathbf{r} + \mathbf{n}L|} - \frac{\operatorname{erf}(\alpha r)}{r} - \frac{\pi}{V\alpha^2} \right], \tag{29}$$

which may be numerically evaluated. In the limit $r \to 0$, we recover the expression

$$\Delta D_{\rm FSC}(r \to 0) = -\frac{k_{\rm B}T}{6\pi\eta} \frac{\xi(r \to 0)}{L},\tag{30}$$

as already derived by Dünweg³³ and Yeh and Hummer,³⁴ where $\xi(r\to 0)\approx 2.837\,297$ is a constant. Equation (30) is frequently used to calculate the finite-size correction for diffusion coefficients obtained from MD simulation data. Similar expressions have been derived for non-cubic box geometries.^{54,55}

Equation (29) may also be converted into its dimensionless form via the dimensionless distance vector \mathbf{r}/L and dimensionless convergence parameter αL ,

$$\Delta D_{\text{FSC}}(r/L) = \frac{k_{\text{B}}T}{6\pi\eta L} \left[\sum_{\mathbf{n}\neq\mathbf{0}} \frac{1}{\pi n^2} \exp\left(2\pi i \,\mathbf{n}\cdot(\mathbf{r}/L)\right) \exp\left(-\frac{\pi^2 n^2}{(\alpha L)^2}\right) \right]$$

$$+ \sum_{\mathbf{n}\neq\mathbf{0}} \frac{\operatorname{erfc}((\alpha L)|(\mathbf{r}/L) + \mathbf{n}|)}{|(\mathbf{r}/L) + \mathbf{n}|}$$

$$- \frac{\operatorname{erf}((\alpha L)(r/L))}{r/L} - \frac{\pi}{(\alpha L)^2} \right]$$

$$= -\frac{k_{\text{B}}T}{6\pi n} \frac{\xi(r/L)}{L}, \tag{31}$$

from which the overall scaling proportional to L^{-1} becomes apparent.

To calculate pair diffusion coefficients expected for the individual terms in Eq. (3) in a periodic MD system, we use $D_{\rm PBC} = D_{\infty} + \Delta D_{\rm FSC}$ for finite r, for which Eq. (31) yields

$$D_{\rm PBC}(r/L) = \frac{k_{\rm B}T}{6\pi\eta L} \left[\frac{L}{r} - \xi(r/L) \right]. \tag{32}$$

Finally, Eq. (11) can be used to convert $D_{\rm PBC}(r)$ to $\rho_{\rm PBC}(r)$ as defined in Eq. (10):

$$\rho_{\rm PBC}(r/L) = \frac{k_{\rm B}T\Delta t}{\pi\eta L} \left[\frac{L}{r} - \xi(r/L) \right]. \tag{33}$$

The numerically evaluated curve for $\xi(r/L)$ is shown in Fig. 6 in Appendix A. We observe that $\xi(r/L)$ slightly decays from its initial value to $\xi \approx 2$ for the largest possible distance in the box, i.e., $r/L = \sqrt{3}/2$. Note that diffusive dynamics has implicitly been assumed in Eq. (33), which we discuss further in Sec. IV.

C. Flow field of the pair diffusion tensor

Rather than taking the trace in Eqs. (26) and (27), we evaluated the flow field generated by the diffusion tensor in Eq. (21) in a first step. Due to the ill-converging behavior of the expression in Eq. (21), we used the Ewald summation in analogy to the derivation of Eq. (28) but retaining the orientational dependence. To this end, the real-space summands [i.e., the second, third and fourth term on the right-hand side of Eq. (29) as well as the expression from Eq. (14)] were weighted by the tensor product $(\Delta \hat{\mathbf{r}}_0 + (\hat{\mathbf{r}} \cdot \Delta \hat{\mathbf{r}}_0)\hat{\mathbf{r}})$, whereas the Fourier term [first term on the right-hand side of Eq. (29)] was scaled by $(\Delta \hat{\mathbf{r}}_0 - (\hat{\mathbf{k}} \cdot \Delta \hat{\mathbf{r}}_0)\hat{\mathbf{k}})$ [cf. tensorial products in Eqs. (14) and (21); see Appendix A for details]. Here, $\Delta \mathbf{r}_0$ is the displacement vector of a point particle in the center of the box, and the hats denote the unit vectors. Unit values and unit vectors have been employed for the numerical evaluation of the flow field.

Figure 3 shows this normalized flow field in the x, y-plane for different $\Delta \mathbf{r}_0$. As already indicated by Fig. 2, we observe a locally aligned flow and a global counterflux in Figs. 3(a) and 3(c) when $\Delta \mathbf{r}_0$ is oriented parallel to the x-axis. Interestingly, when $\Delta \mathbf{r}_0$ acts along the diagonal, vortices appear at large distances from the center in Figs. 3(b) and 3(d). Qualitatively, the flow field in Figs. 3(c) and 3(d) is similar than for the case when $\Delta \mathbf{r}_0$ lies in the x, y-plane [Figs. 3(a) and 3(b)].

D. Comparison with molecular dynamics simulation data

Next, we return to the averaged pair diffusion expressed by Eq. (33), whose predictions are shown in Figs. 2(a) and 2(b) as gray-dashed curves. Note that at this stage, the viscosity entering the

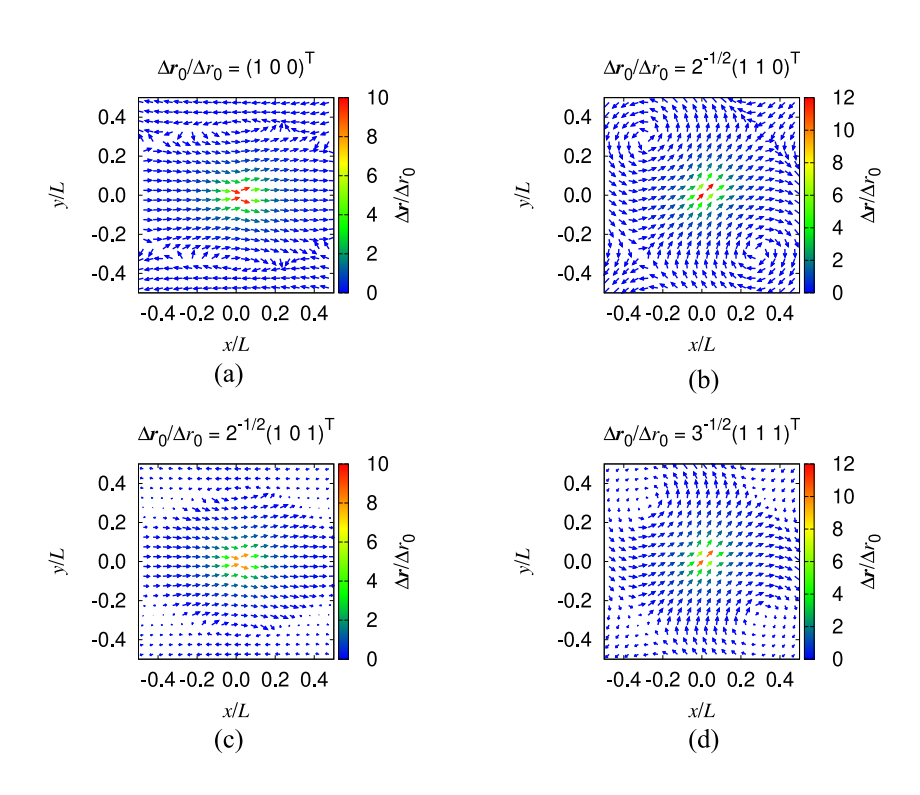


FIG. 3. Normalized flow field generated by the diffusion tensor in Eq. (21) projected onto the x,y-plane for different displacement vectors $\Delta \mathbf{r}_0$ of a point particle in the center of the box. The orientation of the resulting $\Delta \mathbf{r}$ vector field is shown as arrows, and its relative magnitude marked by the color-coding.

prefactor of Eq. (33) has been treated as an empirical fit parameter (see Sec. IV A for a detailed discussion of the role of η). Moreover, a single fit curve only has been determined based on the average of all three MD data curves for a given electrolyte in Fig. 2 (i.e., ρ_{++} , ρ_{+-} , and ρ_{--}). We note an excellent agreement for all pair types for intermediate and large separations ($r \gtrsim 10$ Å), underscoring the universal behavior of the pair diffusion for these distances. Obviously, deviations at short r due to the finite size of the ions and their chemical structure, as well as the oscillating deviations for the IL at somewhat larger distances, are not captured by the analytical prediction due to the assumption of point particles in our theory. Interestingly, similar deviations from ideal behavior have been found for simple hardsphere fluids, ⁵⁶ which have been rationalized by an effective diffusive motion of the particles on a free energy landscape imposed by the local structure of the liquid.⁵⁷ By incorporating the Rotner-Prager finite ion radii could be captured, although accounting for the local ordering appears to be more challenging.

To further probe the impact of the local ordering on the distance dependence observed in Fig. 2, we computed the differences between the $ho_{\rm XY}$ determined from the MD data and the analytical prediction of Eq. (33), i.e., $\Delta \rho_{XY} = \rho_{XY} - \rho_{PBC}$, and compared the resulting differences to the appropriately scaled and shifted radial distribution functions (RDFs, dashed curves). From Figs. 2(c) and 2(d), we observe good agreement of the peak positions of the RDFs and $\Delta \rho_{XY}$ for intermediate r, indicating that the deviations of the MD data from Eq. (33) largely arise from the local electrolyte structure. Notably, for both CE and IL, a qualitative agreement between the RDF peaks and $\Delta \rho_{XY}$ is even found for the first solvation shell $(r \approx 5 \text{ Å})$, although the deviations are somewhat larger for the CE due to its sharp first cation-anion coordination peak in the RDF. Apparently, the ions in the IL can be reasonably approximated as spherical particles, whereas this simplification breaks down for the CE because of the preferential coordination of the small lithium ions to the TFSI oxygen atoms.

Nevertheless, the overall agreement between the MD data and Eq. (33) is fairly good, demonstrating that hydrodynamic interactions significantly govern the cooperative charge transport at larger r. Importantly, these findings, therefore, demonstrate that not only momentum conservation may lead to anticorrelated motion of ions in periodic systems but also the approximate incompressibility of the electrolyte gives rise to hydrodynamic interactions. The incompressibility also rationalizes the locally correlated motion between ions with like charges, as a given ion can only move when its surroundings move in a similar direction. Of course, momentum conservation is present in real systems [hence, the exclusion of the zeroth mode in Eq. (21)] and clearly affects charge transport in ILs, which we will discuss in Sec. IV B. Strikingly, qualitatively similar features as in Fig. 2 have even been observed for polymer electrolytes 15,59,60 (although not the main focus of these studies), again underscoring the universality of hydrodynamic interactions, in line with other analytical calculations.6

IV. TIME DEPENDENCE OF IONIC PAIR DIFFUSION A. Decay of hydrodynamic interactions

So far, diffusive dynamics has been implicitly assumed via Eq. (11). However, the dynamics is still subdiffusive on a time scale

of $\Delta t=30$ ps (CE) and 100 ps (IL), for which the ρ_{XY} in Fig. 2 have been computed. Nonetheless, the agreement between the simulation data and Eq. (33) is already almost quantitative. Of course, the transport properties introduced in Sec. I are usually evaluated for sufficiently large Δt , i.e., the diffusive regime. However, as argued in Sec. III A, the ρ_{XY} -curves become blurred for large Δt due to the fact that the distances between the ions change as Δt increases (in fact, for $\Delta t \to \infty$, ρ_{XY} would even converge to a constant value irrespective of r). On the other hand, for short Δt , ρ_{XY} is well-defined, but the dynamics is still subdiffusive, preventing the evaluation of the contribution of ρ_{XY} to σ_{XY} . Therefore, we characterize the time dependence of ρ_{XY} in more detail in the next step.

Naturally, for larger Δt , the magnitude of ρ_{XY} is larger in the simulations because the ions traveled larger distances on average. Theoretically, space and time dependence of ρ_{XY} are separated in Eq. (33) as the former is given by the universal function $[(L/r) - \xi(L/r)]$, whereas the time dependence is exclusively contained in the prefactor. Although not immediately apparent, not only the linear Δt -term in the prefactor of Eq. (33) but also the short-time viscosity $\eta(\Delta t)$, which is not fully converged in the subdiffusive regime, lend ρ_{XY} its time dependence. In analogy to Eq. (20), we therefore phenomenologically define the short-time viscosity as

$$\eta(\Delta t) = \frac{V}{k_{\rm B}T} \int_0^{\Delta t} dt \langle P_{\beta \gamma}(0) P_{\beta \gamma}(t) \rangle. \tag{34}$$

Details of the calculation of the time-dependent viscosity are given in Appendix C. Figures 4(a) and 4(b) show ρ_{XY} for three different Δt -values normalized by $(k_B T \Delta t)/(\pi \eta(\Delta t)L)$ as expected from Eq. (33) to yield dimensionless quantities. In this way, ρ_{XY} becomes susceptible to dynamical intricacies beyond its trivial dependence on viscosity. In other words, one can assess whether space and time dependence are strictly separated as suggested by Eq. (33). Note that the largest Δt -values in Fig. 4 were chosen such that they are slightly smaller than the onset of the diffusive regime (see below) for reasons mentioned above. In particular, we choose $\Delta t = 3$, 30, and 300 ps for the CE and $\Delta t = 10$, 100, and 1000 ps for the IL.

From Figs. 4(a) and 4(b), we observe the characteristic hydrodynamic behavior for all Δt , that is both on time scales close to the diffusive regime and within the subdiffusive regime down to a few picoseconds. However, with increasing Δt , both the locally positive $(\rho_{XY} > 0)$ and globally negative correlations $(\rho_{XY} < 0)$ diminish in the normalized representation. This can be attributed to the fact that after a certain time, the initial interionic distances r change due to the motion of the ions, resulting in exchange processes within their coordination shells. Consequently, the initial ρ_{XY} values become averaged over different r, leading to the observed decay. This is in agreement with the average distances traveled by the ions during the individual Δt -values as estimated from the mean-squared displacements (MSDs). In particular, for the CE, we find displacements (averaged over both ion species) of 1.2, 2.5, and 6.6 Å for the respective Δt , whereas for the IL, the corresponding values are 1.2, 2.2, and 5.3 Å, the values for the largest Δt being comparable with the ion sizes. As mentioned above, for $\Delta t \rightarrow \infty$, ρ_{XY} would fully decay due to the complete loss of information on the original distances between the different ions. Note that for ILs, this constant would be negative due to momentum conservation (Sec. I). Interestingly,

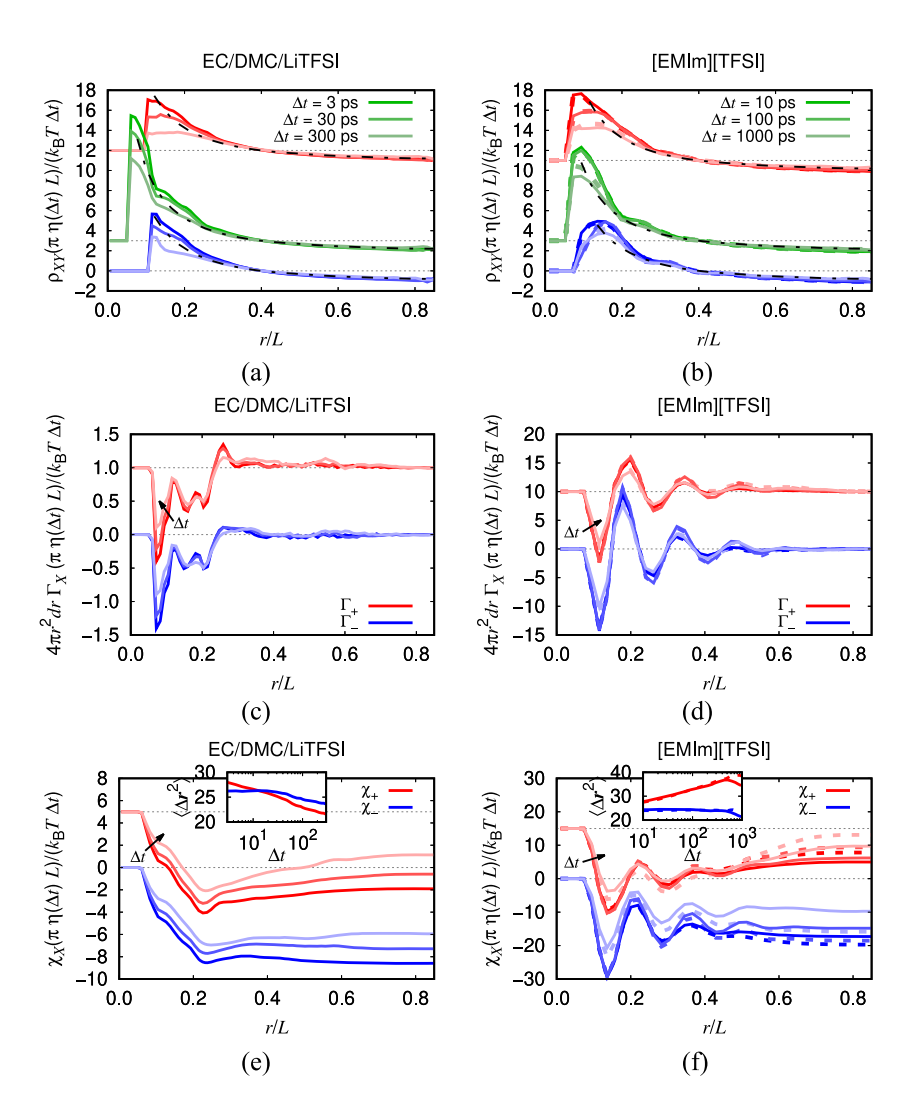


FIG. 4. (a) and (b): Normalized ion correlations $\rho_{\rm XY}$ at different Δt as a function of normalized distance r/L. The color-coding of the pair types is identical to Fig. 2. The dashed-dotted black curves correspond to the prediction from Eq. (33) with time-dependent viscosity $\eta(\Delta t)$ (see text). (c) and (d): Weighted and normalized cross-correlations in the integrand $4\pi r^2\Gamma_{\pm}$ of Eq. (38) (see text). (e) and (f): Integrated and normalized cross-correlations χ_+ and χ_- . The insets of (e) and (f) show the mean squared displacement (MSD) using the same normalization as in the main figures. The dashed lines in (b), (d), and (f) correspond to the ILs with modified masses. The relative uncertainties of the unnormalized plateau values at the largest Δt in (e) and (f) are in the range of 10%. Several curves have been shifted for better visibility.

in the opposite limit $\Delta t \rightarrow 0$, the velocities should obey the Maxwell-Boltzmann distribution such that the velocities/displacements of two ions are uncorrelated irrespective of their distance. Thus, also in the short-time limit, ρ_{XY} would be a constant (which is negative for ILs due to residual correlations satisfying momentum conservation²⁸). However, from Figs. 4(a) and 4(b), we find that starting from a few picoseconds, the hydrodynamic picture already holds. This is also reflected by the comparison with the theoretical curve [Eq. (33), black dashed-dotted lines in Figs. 4(a) and 4(b); unlike in Fig. 2, the curves were only normalized, but no fitting was performed]. For both electrolytes, we find that for short Δt , the magnitude of ρ_{XY} is larger than the prediction by about 10%-30% for all except short r, for which the comparison breaks down due to the local structure. Keeping in mind that the dynamics only becomes diffusive at the respective largest Δt , larger ρ_{XY} -values in the MD simulations are not surprising as it is generally observed that when applying Eq. (12) (or the corresponding equation for pair diffusion) in the subdiffusive regime, the resulting approximate (pair) diffusion coefficients are larger than their long-time values (see Fig. 5 in Sec. IV C below). However, as argued above, ρ_{XY} decays due to structural

rearrangements in the opposite limit $\Delta t \to \infty$. In this context, it is important to stress a subtle difference between the definition of ρ_{XY} as extracted from the MD data and the hydrodynamic theory in Sec. III B: Eq. (33) was derived on the basis of a continuous flow field [see for example Eqs. (15) or (22)]; therefore, the pair diffusion coefficient is determined for a fixed distance r between two points within the periodic cell. On the contrary, the interionic distance in the MD simulations evolves with time, which ultimately leads to the complete decay of ρ_{XY} . Implications of this conceptual difference can indeed be observed from Figs. 4(a) and 4(b): Although Eq. (33) predicts that space and time dependence can be separated, the MD curves still show a residual time dependence (i.e., their decay) despite the normalization by the prefactor of Eq. (33), which theoretically contains the entire time dependence. At the onset of the diffusive regime, the average displacement of the ions becomes comparable with their own size or the size of their solvation shell² (~5 Å), which is still small compared with the large and intermediate distances in Figs. 4(a) and 4(b). Consequently, we observe that the hydrodynamic picture is still valid for the largest Δt values before the trivial long-time decay continues. For the largest Δt values, we

find that the MD curves in Figs. 4(a) and 4(b) match the prediction from Eq. (33) almost quantitatively for larger r. Several factors could contribute to this coincidence: First, the pair diffusion coefficients are no longer overestimated as in the subdiffusive regime; second, Eq. (34) converges to the constant long-time viscosity and thus becomes equivalent to Eq. (20); and finally, the ion displacements are still comparatively small to the interionic distances on which hydrodynamic interactions are relevant.

It is also worth noting that the ρ_{XY} are similar to the coupling factor λ defined in our recent work on IL/Li-salt mixtures.²² In particular, λ expresses the degree of coupled diffusion between the displacement vectors of initially neighbored ions, similar in spirit to a correlation coefficient. For IL/Li-salt mixtures, we observed a large degree of coupled diffusion for small salt concentrations ($\lambda \approx 0.8$) due to the stable lithium coordination shell composed of anions.² Conversely, substantially smaller values for λ were found at high concentrations because anions are shared between distinct lithium ions as coordination partners. Consistent with the alternating structure of cations and anions in pure ILs studied in this work, leading to shared coordination partners as well, one would expect a moderate albeit significant degree of coupled diffusion. Indeed, when normalizing ρ_{xy} by the MSDs in analogy to λ , we find values of 0.35 for the first coordination sphere of the IL. For the CE, this value is significantly larger (\sim 0.6) as expected from the lower ion concentration such that shared coordination shells composed of one anion and two cations (or vice versa) hardly emerge. This is also in line with a recent analysis showing that in CEs the transport mainly occurs in a vehicular fashion, i.e., collectively with the local environment. 63 Moreover, in our previous work, we found that λ decays with increasing time due to the fact initially nearby ions disengage,²² compatible with the present observations from Figs. 4(a) and 4(b). Nonetheless, we found previously that even after a neighboring ion left a given ion's coordination sphere, some residual dynamical coupling persists as a result of the hydrodynamic flow field.²² The hydrodynamic theory developed in Sec. III fully rationalizes these earlier findings, as it accounts for any interionic distance.

Finally, Fig. 4(b) also shows the respective normalized ρ_{XY} -curves for the systems in which the ion masses have been scaled (Sec. II) as dashed lines. Although the differences compared with the original systems appear to be minute for ρ_{XY} , they will turn out to be crucial for the contributions to σ_{XY} (Sec. IV B).

B. Implications for the conductivity

Next, we discuss how the electrolyte structure, the hydrodynamic flow field, as well as the deviations from it govern σ_+ and σ_- . More generally, to relate ρ_{XY} and σ_{XY} , we express Eq. (4) as

$$\sigma_{XY}(\Delta t) = \frac{e^2 N_X}{6V k_B T \Delta t} \left[\langle \Delta \mathbf{r}^2 (\Delta t) \rangle_X \, \delta_{XY} + \frac{z_X z_Y (N_Y - \delta_{XY})}{V} \right] \times \int_V d\mathbf{r} \, \rho_{XY}(r, \Delta t) \, g_{XY}(r) , \qquad (35)$$

in analogy to early analytical work^{48–51,64} and recent simulation studies.^{28–30} Here, $g_{XY}(r)$ denotes the RDF between ion species X and Y, $\langle \Delta \mathbf{r}^2(\Delta t) \rangle_X$ is the MSD of species X during Δt , and δ_{XY} is the Kronecker delta. For $\sigma_X = \sigma_{XX} + \sigma_{XY}$, we rewrite Eq. (6) as

$$\sigma_X(r,\Delta t) = \frac{e^2 N_X}{6V k_{\rm B} T \Delta t} \left[\langle \Delta \mathbf{r}^2(\Delta t) \rangle_X + \chi_X(r,\Delta t) \right], \tag{36}$$

where the first term on the right-hand side is the ideal Nernst-Einstein conductivity,

$$\sigma_{X,0}(\Delta t) = \frac{e^2 N_X D_X(\Delta t)}{V k_B T},$$
(37)

arising from the self-diffusion of species X [Eq. (12)] and

$$\chi_{X}(r,\Delta t) = \int_{0}^{r} dr' \, 4\pi r'^{2} \, \frac{N_{X}}{V} \left[\frac{N_{X} - 1}{N_{X}} \rho_{XX}(r',\Delta t) \, g_{XX}(r') - \rho_{XY}(r',\Delta t) \, g_{XY}(r') \right]$$

$$= \int_{0}^{r} dr' \, 4\pi r'^{2} \, \Gamma_{X}(r',\Delta t), \tag{38}$$

is a short-hand notation for the distance-dependent cross-correlations experienced by ions of type X. In Eq. (38), we expressed χ_X as a function of the upper bound r of the integral. Although spherical integration can be carried out due to isotropy, it should be emphasized that the integral in Eq. (35) also contains contributions for $L/2 < r \le \sqrt{3}L/2$, for which $g_{XY}(r) < 1$.

For ideal structureless electrolytes with $g_{XY}(r) = 1$ and $\rho_{XY}(r) = 1$ strictly given by Eq. (33) (i.e., no deviations as observed in Fig. 2), $\chi_{\rm x}$ would be zero when integrated over the entire box because the integral over Eq. (28) vanishes [this is most easily seen when performing the integration of the analogous Eq. (27) for all three spatial components separately].^{53,65} However, even for a real electrolyte, it is obvious from Figs. 4(a) and 4(b) and Eq. (38) that when calculating χ_+ and χ_- , the hydrodynamic interactions contained in, say, ρ_{++} will largely cancel with those of ρ_{+-} . That is only when either ρ_{XY} is non-ideal (Fig. 2) or when $g_{XY} \neq 1$, remaining contributions to χ_{\pm} can be expected when subtracting the two integrands in Eq. (38). Before embarking on the discussion of χ_{+} , it is therefore instructive to consider the difference of the two integrands in Eq. (38), denoted as Γ_{\pm} and weighted by $4\pi r^2$ due to radial symmetry [Figs. 4(c) and 4(d); the same normalization as for ρ_{XY} has been applied]. We find that for both the CE and the IL, the non-vanishing non-hydrodynamic contribution at short distances is negative (i.e., decreasing the overall conductivity) due to the preferential interactions of oppositely charged ions on a local scale. However, although for the CE only marginal contributions are observed for $r/L \gtrsim 0.3$ [Fig. 4(c)], several additional peaks occur up to a distance of r/L \lesssim 0.6 for the IL [Fig. 4(d)]. As expected from the decay of ρ_{XY} for larger Δt , the magnitude of the non-vanishing cross-correlations decreases for both the CE and the IL. The dashed curves in Fig. 4(d) again show the results for the IL with modified ion masses. As in Fig. 4(b), these differences appear to be minute but will turn out to be significant on integration via Eq. (38), which we will study next.

Figures 4(e) and 4(f) show the integrated χ_{\pm} as a function of the upper bound of the integral in Eq. (38) with the same normalization as before. As already expected from Figs. 4(c) and 4(d), the negative contribution at short distances is dominating, such that the entire integral is smaller than zero for all r (note that the χ_{+} -curves have been shifted for clarity). Although this behavior is encountered for both electrolytes, only the IL shows significant contributions beyond local scales, again reflected by multiple peaks arising from

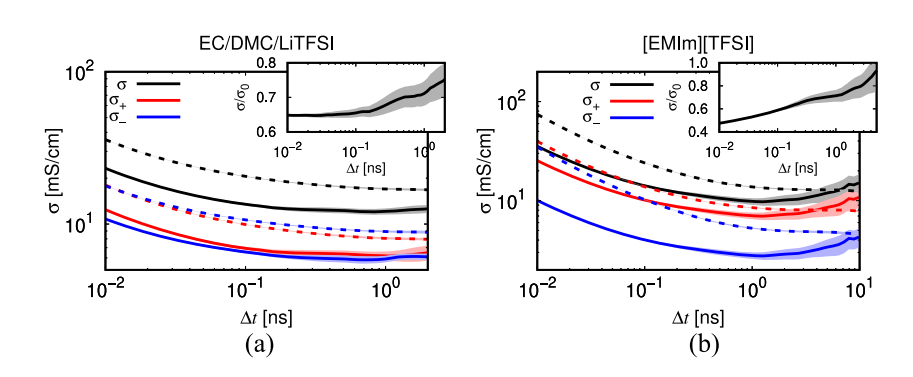


FIG. 5. Time-dependent conductivities (solid lines) and ideal Nernst-Einstein conductivities (dashed lines) for (a) CE and (b) IL. The standard deviations are indicated as shaded regions. The degree of uncorrelated ion motion, expressed as σ/σ_0 , is shown in the insets (note that for large Δt , the uncertainties become large such that the estimation of σ/σ_0 becomes challenging).

the rather long-ranged ordering. By contrast, χ_{-} is approximately constant for $r/L \gtrsim 0.4$ in the case of the CE, whereas χ_{+} still displays minor changes for larger r/L, probably due to a minor ordering of the ions on these scales. Another interesting IL-specific effect can be observed at large r from Fig. 4(f): Here, χ_{+} still changes slightly for r/L > 0.6. By comparison with the curves of the IL with modified masses (dashed curves), it becomes obvious that this is an imprint of the momentum-conservation constraint, as the correlated ionic motion at more local scales has to be globally compensated (Sec. I). A similar observation can be made for the second IL studied here, [EMIm][BF₄], which is shown in Appendix B [Fig. 7(e)]. With increasing Δt , the magnitude of the peaks of χ_{\pm} decreases for both CE and IL due to local relaxation processes as already observed from Figs. 4(c) and 4(d).

Interestingly, also the plateau values of χ_+ at $r/L \rightarrow \sqrt{3}/2$, reflecting the overall cross-correlations, decrease with increasing Δt , demonstrating that not all dynamical features in the subdiffusive regime are captured by $\eta(\Delta t)$. A similar finding was already made in the context of Figs. 4(a) and 4(b): Unlike the hydrodynamic theory based on a continuous flow field, the distances between discrete ions in the simulation relax with time, which additionally contributes to their mutual pair diffusion. Apparently, the residual time dependence of $\rho_{XY}(\Delta t)$ not contained in $\eta(\Delta t)$ [Figs. 4(a) and 4(b)] does not entirely vanish when performing the integration according to Eq. (38) despite locally positive and globally negative correlations. In particular, for CE, the magnitude of $\chi_+^{\rm int} = \chi_+(r/L \to \sqrt{3}/2)$ decreases by about 40% and the corresponding $\chi_{-}^{\rm int}$ decreases by a comparable amount of 30% when going from 3 to 300 ps. Due to the fact that χ_{\pm}^{int} is negative and hence decreasing both σ_{\pm} and σ_{τ} its decrease in magnitude because of the additional relaxation processes enhances the conductivity. In other words, if the dynamics was entirely governed by $\eta(\Delta t)$, $\chi_{\pm}^{\rm int}$ would remain constant, leading to lower σ values for longer Δt . However, the decrease of $|\gamma_{+}^{\text{int}}|$ is overcompensated by an increase of $\eta(\Delta t)$ by 130% between 3 and 300 ps, contributing to the fact that $\sigma(\Delta t)$ decreases with increasing Δt in the subdiffusive regime (see below). For the IL, the magnitude of $\chi_{+}^{\rm int}$ and $\chi_{-}^{\rm int}$ decreases by 40%–50% when going from 10 to 1000 ps, whereas $\eta(\Delta t)$ increases by a factor of almost six. This indicates that although the relaxation of the electrolyte structure affects χ_{\pm}^{int} and thus the conductivity value, the high viscosity of ILs slows down the ionic motion more strongly compared with other electrolytes.

In the case of ILs, the Δt -dependence of $\chi_{\pm}^{\rm int}$ is influenced by momentum conservation. This is best seen from the comparison

of [EMIm][TFSI] and [EMIm][BF₄]: For [EMIm][TFSI], the value decreases for $\chi_+^{\rm int}$ and $\chi_-^{\rm int}$ with increasing Δt , both with standard and with modified masses [Fig. 4(f)]. Although the same behavior is found for [EMIm][BF₄] for standard masses, the trend becomes reverted for $\chi_+^{\rm int}$ when the masses are scaled [Fig. 7(e)]. In this context, it is noteworthy that by our scaling procedure, the anions become heavier than the cations for [EMIm][BF₄], whereas the opposite is true for standard molar masses. For [EMIm][TFSI]; however, the cations are lighter than the anions in both cases. One may therefore speculate that the compensation of the local exchange processes by the motion of remote ions is affected by these details.

C. Self-diffusion and cross-correlation

Naturally, apart from the integrated cross-correlations χ_{+}^{int} , the self-diffusion of the ions contributes a large fraction to the total conductivity. In practice, one, therefore, usually aims not only to either increase the mobility of the ions (often the cation) but also to alter the ionic correlations by employing different salts or solvents to optimize an electrolyte. 1,2 The insets in Figs. 4(e) and 4(f) show the ions' MSDs with the same normalization as for $\chi_{\pm}^{\rm int}$, making both quantities directly comparable. As for the cross-correlations, we observe that not all dynamical features affecting the subdiffusive regime are captured by $\eta(\Delta t)$, reflected by an additional Δt -dependence in Figs. 4(e) and 4(e). In particular, both curves become slightly smaller for the CE, whereas in the case of the IL, the cationic contribution increases, whereas the anionic contribution remains constant. This shows that at least for certain ionic species, additional short-time processes, e.g., arising from local relaxation processes, the ions' internal degrees of freedom or forward-backward correlations, affect the MSDs in a different fashion than the collective property $\eta(\Delta t)$. However, this apparent deviation from the simplified Stokes-Einstein relation is not too surprising. From experimental works and simulations, it is known that the Stokes-Einstein relation provides a reasonable first estimate, although deviations of about a factor of two are commonly observed.⁶ Interestingly, however, both the MSD and $\eta(\Delta t)$ remain unaffected within the uncertainties when changing the masses [dashed curves Figs. 4(e) and 4(f) as well as Appendix C], consistent with the overdamped dynamics in a highly viscous medium that is commonly assumed.

Finally, Fig. 5 shows the conductivities σ_X together with ideal Nernst-Einstein conductivities $\sigma_{X,0}$ [Eq. (37)]. Importantly, due to

momentum conservation, $\sigma_+/\sigma_- = m_-/m_+$ for the IL (Sec. I). However, as evident from Figs. 4(e) and 4(f), the product $\chi_{\pm}^{int}(\Delta t) \eta(\Delta t)$ is not strictly constant, which implies that also the diffusion coefficients contained in $\sigma_{X,0}$ cannot be fully governed by $\eta(\Delta t)$, as otherwise $\sigma_+/\sigma_- \neq \text{const}$ [cf. Eq. (36)]. Notably, the additional dynamical contributions not contained in $\eta(\Delta t)$ and affecting self-diffusion and cross-correlations in a different way have important technical implications for MD simulations: The ratio σ/σ_0 , also termed degree of uncorrelated motion, which is frequently used to quantify the deviations from the Nernst-Einstein behavior, 17,67,68 itself is time-dependent, at least for the CE and the ILs studied in this work [see insets of Figs. 5(a) and 5(b)]. Due to the fact that the uncertainties of σ_0 are considerably smaller than those of σ (the former can be averaged over all N ions in the system, leading to uncertainties roughly lower by a factor of \sqrt{N}), 15,69 one might be tempted to determine σ/σ_0 on short subdiffusive scales and then using this ratio in combination with the statistically more robust σ_0 to extrapolate σ to the diffusive regime. However, our observations from Fig. 5 show that such an approach is generally not valid because σ/σ_0 varies between 0.5 and 0.7 at $\Delta t = 10$ and 1000 ps, respectively, for the IL. For the CE, the variation in σ/σ_0 is smaller albeit significant. Therefore, extrapolation from short Δt would underestimate the true σ . Consequently, the explicit calculation of σ is

In total, our findings demonstrate that the pair-diffusion contribution to the conductivity is affected by at least two dynamical features: First, hydrodynamic interactions largely govern the overall dynamics of the system. Apart from the electrolyte structure affecting the precise value of the hydrodynamic integral, the viscosity is a key parameter characterizing these interactions, in line with the well-known Walden picture 17,19,70-72 and recent MD results.73 Second, however, relaxation processes, leading to changes in the interionic distances, give rise to additional dynamical contributions that are not captured by the hydrodynamic theory. For the electrolytes studied in this work, these deviations lead to an enhancement of the overall conductivity, although it is unclear whether this is generally the case. Although the importance of hydrodynamic interactions was already recognized in early analytical treatments of ionic conductivity, 48-51 the deviations observed in this work are more intricate but can be probed by simulations. In this context, it is also noteworthy that it has recently been speculated for CEs that the local viscosity of the environment around an ion or a solvate structure rather than the global viscosity is important for diffusion.63 Similar local friction effects have been discussed in the

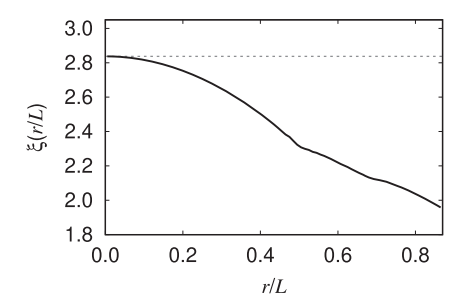


FIG. 6. Distance dependence of the finite-size correction $\xi(r/L)$ in Eq. (33).

context of the structural relaxation of ILs. ^{74,75} It seems plausible that such local viscous effects are relevant for the pair diffusion as well. This is even more reasonable as our current theory is based on a single-component fluid with point particles. Theories describing hydrodynamic flow in multicomponent systems ^{76,77} or finite ion radii ^{31,58} thus are possible extensions of the model. Nevertheless, the present work shows that the hydrodynamic picture holds a very good approximation until the onset of the diffusive regime. In puresalt electrolytes such as ILs, the pair diffusion is also affected by momentum conservation. A similar effect is expected for highly concentrated binary electrolytes (i.e., salt and solvent). ^{78,79} Through a detailed analysis, the distinct contributions can be disentangled to deliberately optimize the electrolytes.

V. CONCLUSIONS AND OUTLOOK

In this paper, we presented an analytical theory describing the distance dependence of pair diffusion in periodic systems. Essentially, due to the incompressibility of the medium, our theory predicts locally correlated motion, which is compensated by a counterflux at large distances. We find very good agreement between the analytical prediction and the distance dependence of dynamical ion correlations in ILs extracted from MD simulation data, although noticeable deviations occur due to several different reasons: First, the local structure of the electrolyte and the resulting effective potentials acting on the ions give rise to deviations from the theoretical prediction at short distances. Second, on larger time scales, the relaxation of the electrolyte structure leads to the decay of the hydrodynamic interactions. Finally, for ionic liquids, the physical constraint of momentum conservation acts on larger length scales. Despite this important constraint, our theory shows that the anticorrelated motion occurring for ionic liquids at large distances in periodic systems can be largely rationalized by hydrodynamic interactions arising from the incompressibility of the electrolyte. Consequently, the same qualitative behavior is observed for electrolytes including a neutral solvent.

The decay of the hydrodynamic interactions is largely governed by the viscosity, in line with the well-known Walden picture. ^{17,19,70-72} However, the relaxation of the electrolyte structure is not captured by the hydrodynamic theory such that significant deviations arise that affect the ionic cross-correlations. Nonetheless, the hydrodynamic picture remains valid until the dynamics becomes diffusive. Via our framework, it is possible to separate the relative importance of hydrodynamic effects and relaxation, which—in addition to the electrolyte structure—govern the collective dynamics between distinct ions. Because quantitatively different deviations occur for the self-diffusion, the degree of uncorrelated motion becomes time-dependent in the subdiffusive regime.

From the perspective of battery science and electrochemistry, incorporating electrode interfaces into the formalism, in analogy to recent work on self-diffusion near interfaces, ⁸⁰ is another promising avenue. In this context, it also seems worthwhile to scrutinize a recent hypothesis according to which in concentrated electrolytes confined between two electrodes, the transport parameters are governed by volume rather than momentum conservation. ⁸¹ Finally, our theoretical formalism likely also provides insights into the finite-size effects of ionic correlations. Recently, Shao *et al.* ⁷³ have shown

numerically that although the diffusion coefficients show their well-known finite-size effects^{33–35} proportional to L^{-1} , the overall conductivity is independent of the system size, implying that the cross-correlations must exhibit finite-size effects that compensate the finite-size effect of the diffusivity. Indeed, a finite-size effect proportional to L^{-1} was found from their MD simulations for the cross correlations.⁷³ Similar empirical observations have been made for mutual diffusivities in multicomponent systems. 82,83 Jamali et al. 82 found that the finite-size correction for Maxwell-Stefan diffusivities differs from that of the self-diffusion coefficients by a factor equal to the inverse thermodynamic factor. From Eq. (33), we recognize that the correction to the pair diffusion scales inversely with both the viscosity as well as the box length, similar to that of self-diffusion coefficients. 33-35 As demonstrated by Jamali et al., 82 the impact of the structure of the liquid on the pair (or mutual) diffusion could be captured by the thermodynamic factors, which we leave for future analyses.

ACKNOWLEDGMENTS

The authors thank Gerhard Hummer, Jens Smiatek, and Volker Lesch for helpful discussions.

AUTHOR DECLARATIONS

Conflict of Interest

The authors have no conflicts to disclose.

Author Contributions

Diddo Diddens: Conceptualization (equal); Data curation (lead); Formal analysis (equal); Validation (equal); Writing – original draft (lead); Writing – review & editing (equal). **Andreas Heuer**: Conceptualization (equal); Data curation (supporting); Formal analysis

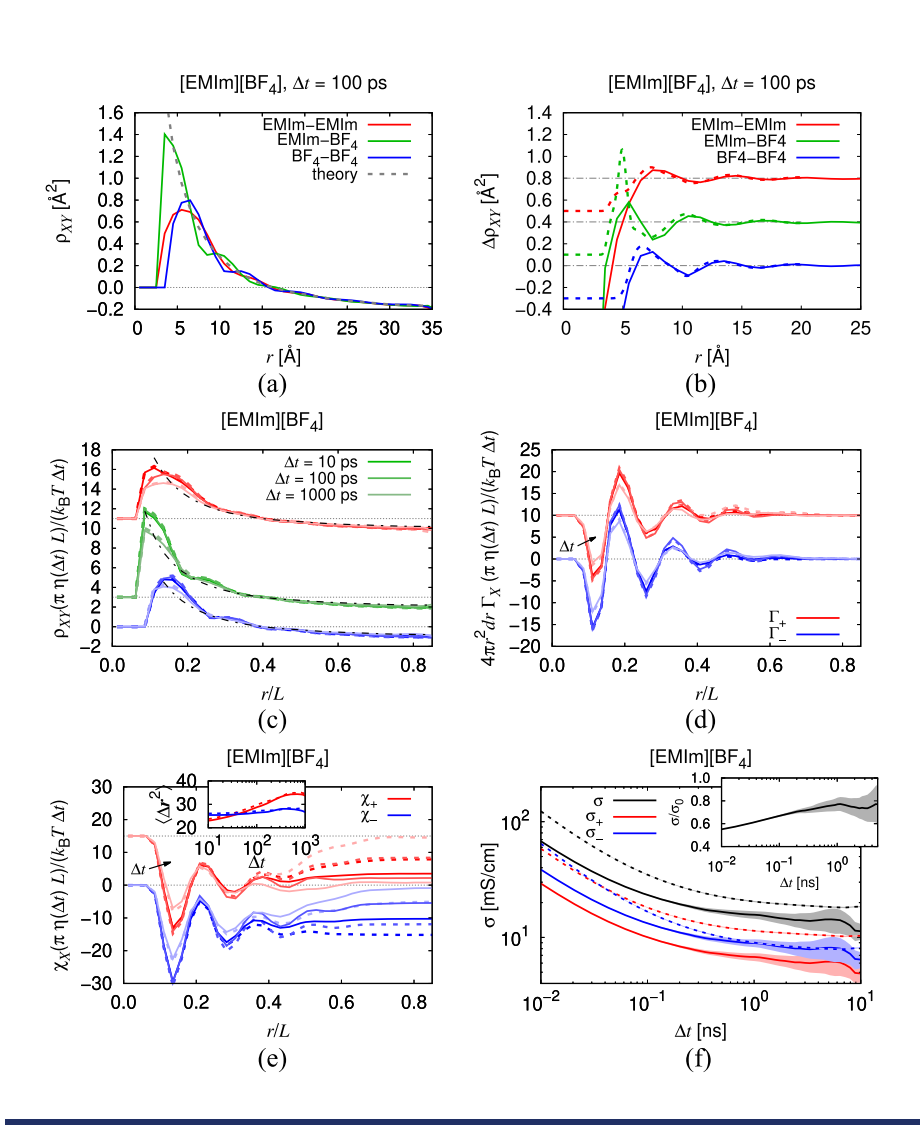


FIG. 7. Results for [EMIm][BF₄]. (a): Distance-dependent correlation $\rho_{XY}(r)$ together with hydrodynamic fit (dashed), (b): deviations of the simulation data from the hydrodynamic fit (solid) with the scaled and shifted RDFs (dashed), (c): normalized $\rho_{\rm XY}$ at different Δt as a function of normalized distance r/L together with the theory curve (dashed-dotted), (d): weighted and normalized crosscorrelations $4\pi r^2\Gamma_{\pm}$, (e): integrated and normalized cross-correlations $\chi_{\pm},$ and (f): time-dependent conductivities (solid) and ideal Nernst-Einstein conductivities (dashed). Several curves have been shifted for better visibility.

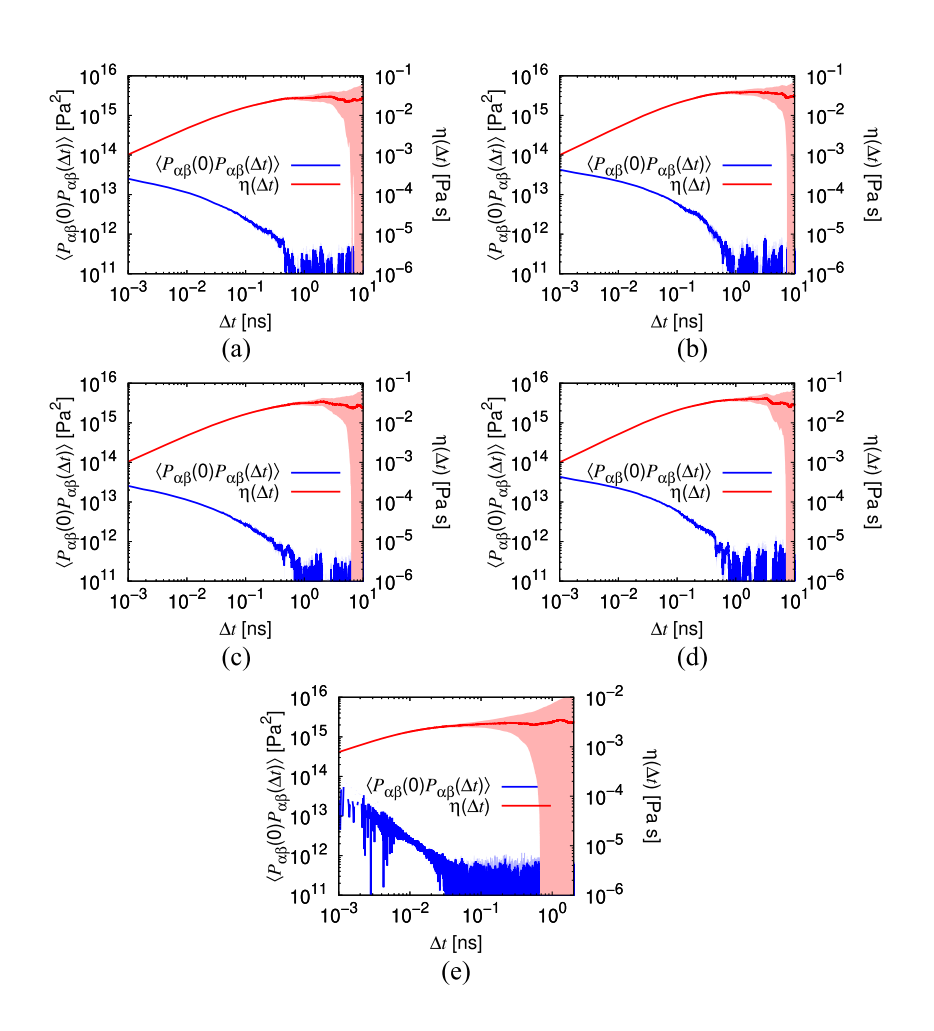


FIG. 8. Pressure tensor autocorrelation function $\langle P_{\beta\gamma}(0)P_{\beta\gamma}(t)\rangle$ and time-dependent viscosity $\eta(t)$ determined from the cumulative integral in Eq. (34) for (a) [EMIm][TFSI] and (b) [EMIm][BF₄] with ordinary masses; (c) [EMIm][TFSI] and (d) [EMIm][BF₄] with modified masses (Sec. II) as well as (e) EC/DMC/LiTFSI.

(equal); Validation (equal); Writing – original draft (supporting); Writing – review & editing (equal).

DATA AVAILABILITY

The data that support the findings of this study are available from the corresponding author upon reasonable request.

APPENDIX A: NUMERICAL EVALUATION OF THE EWALD SUM

The distance dependence of $\xi(r/L)$ in Eq. (33) was evaluated numerically (Fig. 6). To this end, the convergence parameter α has been chosen such that both the summation in real space and in reciprocal space in Eq. (31) converged with a reasonable number of lattice vectors (30 vectors in each spatial direction in our case), which, in practice, corresponds to a value of αL on the order of one. The orientation of the distance vector \mathbf{r} has been sampled randomly and the lattice sums in Eq. (31) have been carried out for all three dimensions. We note that for $r \to 0$, we recover the numerical value of $\xi \approx 2.837$ 297 reported previously. ^{33,34} For larger distances, ξ is a slowly varying function of r, and decays to about 70% of its original value for $r/L = \sqrt{3}/2$. Slight kinks can be observed at r/L = 1/2

(maximum distance in one spatial direction) and $r/L = \sqrt{2}/2$ (maximum distance within a plane defined by any two spatial directions). Due to the fact that the above derivation approximates the particles as point-like, no further length scale like the particle radius enters the distance dependence shown in Fig. 6.

For the orientation-dependent flow fields $\Delta \mathbf{r}_{PBC}(\hat{\mathbf{r}},r/L)$ in Fig. 3, we carried out analogous lattice sums but retained the orientational dependence expressed by the tensor products. In particular, all real-space terms have been weighted by the tensor product $(\Delta \hat{\mathbf{r}}_0 + (\hat{\mathbf{r}} \cdot \Delta \hat{\mathbf{r}}_0)\hat{\mathbf{r}})$, whereas the term evaluated in reciprocal space was weighted by $(\Delta \hat{\mathbf{r}}_0 - (\hat{\mathbf{k}} \cdot \Delta \hat{\mathbf{r}})\hat{\mathbf{k}})$ (with $\Delta \mathbf{r}_0$ being the displacement vector of a particle in the center of the box:

$$\begin{split} \Delta \mathbf{r}_{PBC}(\hat{\mathbf{r}},r/L) &= \frac{3}{4} \frac{k_B T \Delta t}{\pi \eta L} \bigg[(\Delta \hat{\mathbf{r}}_0 + (\hat{\mathbf{r}} \cdot \Delta \hat{\mathbf{r}}_0) \hat{\mathbf{r}}) \bigg(\frac{L}{r} \bigg) \\ &+ \sum_{\mathbf{n} \neq \mathbf{0}} \frac{2 \Big(\Delta \hat{\mathbf{r}}_0 - (\hat{\mathbf{k}} \cdot \Delta \hat{\mathbf{r}}_0) \hat{\mathbf{k}} \Big)}{\pi n^2} \exp \big(2\pi i \, \mathbf{n} \cdot (\mathbf{r}/L) \big) \\ &\times \exp \bigg(- \frac{\pi^2 n^2}{(\alpha L)^2} \bigg) + (\Delta \hat{\mathbf{r}}_0 + (\hat{\mathbf{r}} \cdot \Delta \hat{\mathbf{r}}_0) \hat{\mathbf{r}} \big) \end{split}$$

$$+ \left(\sum_{\mathbf{n} \neq \mathbf{0}} \frac{\operatorname{erfc}((\alpha L)|(\mathbf{r}/L) + \mathbf{n}|)}{|(\mathbf{r}/L) + \mathbf{n}|} - \frac{\operatorname{erf}((\alpha L)(\mathbf{r}/L))}{\mathbf{r}/L} - \frac{\pi}{(\alpha L)^2} \right) \right]. \tag{A1}$$

Unit values have been chosen for $k_B T$, Δt , η , and L in Fig. 3, and all vectors have been normalized to unit vectors.

APPENDIX B: COMPARISON WITH [EMIm][BF4]

In addition to [EMIm][TFSI], the IL [EMIm][BF₄] has been simulated as well. The analogous results are summarized in Fig. 7. We observe that the results are qualitatively the same as for [EMIm][TFSI].

APPENDIX C: VISCOSITY CALCULATION

To compute the prefactor in Eq. (33), the viscosity was extracted from the MD data via the autocorrelation function of the pressure tensor^{34,52} [Eqs. (20) and (34)]. Fig. 8 shows $\langle P_{\beta \nu}(0) P_{\beta \nu}(\Delta t) \rangle$ and the corresponding integral according to the Green-Kubo relation in Eq. (34). We note that for the ILs starting from around 500 ps, the statistics deteriorates. Nonetheless, since absolute value of $\langle P_{\beta \nu}(0) P_{\beta \nu}(\Delta t) \rangle$ is small for $\Delta t > 500$ ps, the uncertainties of the corresponding cumulative integrals (shaded areas in Fig. 8) are acceptable until a few nanoseconds, at which $\eta(\Delta t)$ converges to its long-time value. The long-time viscosity was estimated at $\Delta t = 1$ ns for both ILs, where the integral of Eq. (34) saturates. We obtain $\eta = 27.3 \pm 3.9$ mPa s for [EMIm][TFSI] and $\eta = 38.1 \pm 4.4$ mPa s for [EMIm][BF₄] at $\Delta t = 1$ ns. For the ILs with modified masses, we find corresponding values of 31.5 ± 3.8 and 38.4 ± 3.6 mPa s for [EMIm][TFSI] and [EMIm][BF₄], respectively. For larger Δt -values no further trend for $\eta(\Delta t)$ can be identified within the uncertainties. Remarkably, the viscosities for the ILs with modified masses are identical to those of the standard ILs, showing that the potential (mainly electrostatic) terms in Eq. (19) outweight the kinetic terms. For the CE, the statistics deteriorates from about Δt > 100 ps. The estimated long-time viscosity at $\Delta t = 300$ ps is 3.0 ± 1.3 mPa s.

REFERENCES

- ¹ K. Xu, "Nonaqueous liquid electrolytes for lithium-based rechargeable batteries," Chem. Rev. **104**, 4303–4418 (2004).
- ²K. Xu, "Electrolytes and interphases in Li-ion batteries and beyond," Chem. Rev. 114, 11503–11618 (2014).
- ³G. Gebresilassie Eshetu, M. Armand, B. Scrosati, and S. Passerini, "Energy storage materials synthesized from ionic liquids," Angew. Chem., Int. Ed. 53, 13342–13359 (2014).
- ⁴M. Watanabe, M. L. Thomas, S. Zhang, K. Ueno, T. Yasuda, and K. Dokko, "Application of ionic liquids to energy storage and conversion materials and devices," Chem. Rev. 117, 7190–7239 (2017).
- ⁵M. Gouverneur, J. Kopp, L. van Wüllen, and M. Schönhoff, "Direct determination of ionic transference numbers in ionic liquids by electrophoretic NMR," Phys. Chem. Chem. Phys. 17, 30680–30686 (2015).
- ⁶M. Brinkkötter, G. A. Giffin, A. Moretti, S. Jeong, S. Passerini, and M. Schönhoff, "Relevance of ion clusters for Li transport at elevated salt concentrations in [Pyr₁₂₀₁][FTFSI] ionic liquid-based electrolytes," Chem. Commun. **54**, 4278–4281 (2018).

- ⁷A. Hosseinioun, P. Nürnberg, M. Schönhoff, D. Diddens, and E. Paillard, "Improved lithium ion dynamics in crosslinked PMMA gel polymer electrolyte," RSC Adv. 9, 27574–27582 (2019).
- ⁸M. P. Rosenwinkel, R. Andersson, J. Mindemark, and M. Schönhoff, "Coordination effects in polymer electrolytes: Fast Li⁺ transport by weak ion binding," J. Phys. Chem. C **124**, 23588–23596 (2020).
- ⁹S. Pfeifer, F. Ackermann, F. Sälzer, M. Schönhoff, and B. Roling, "Quantification of cation–cation, anion–anion and cation–anion correlations in Li salt/glyme mixtures by combining very-low-frequency impedance spectroscopy with diffusion and electrophoretic NMR," Phys. Chem. Chem. Phys. 23, 628–640 (2021).
- ¹⁰P. Nürnberg, J. Atik, O. Borodin, M. Winter, E. Paillard, and M. Schönhoff, "Superionicity in ionic-liquid-based electrolytes induced by positive ion-ion correlations," J. Am. Chem. Soc. 144, 4657–4666 (2022).
- ¹¹S. Zugmann, M. Fleischmann, M. Amereller, R. M. Gschwind, H. D. Wiemhöfer, and H. J. Gores, "Measurement of transference numbers for lithium ion electrolytes via four different methods, a comparative study," Electrochim. Acta 56, 3926–3933 (2011).
- ¹²F. Wohde, M. Balabajew, and B. Roling, "Li⁺ transference numbers in liquid electrolytes obtained by very-low-frequency impedance spectroscopy at variable electrode distances," J. Electrochem. Soc. 163, A714 (2016).
- ¹³N. M. Vargas-Barbosa and B. Roling, "Dynamic ion correlations in solid and liquid electrolytes: How do they affect charge and mass transport?," ChemElectroChem 7, 367–385 (2020).
- 1⁴P. G. Bruce, J. Evans, and C. A. Vincent, "Conductivity and transference number measurements on polymer electrolytes," Solid State Ionics 28–30, 918–922 (1988).
 1⁵F. Müller-Plathe and W. F. van Gunsteren, "Computer simulation of a polymer electrolyte: Lithium iodide in amorphous poly(ethylene oxide)," J. Chem. Phys. 103, 4745–4756 (1995).
- ¹⁶D. R. Wheeler and J. Newman, "Molecular dynamics simulations of multicomponent diffusion. 1. Equilibrium method," J. Phys. Chem. B 108, 18353–18361 (2004).
- ¹⁷K. Oldiges, D. Diddens, M. Ebrahiminia, J. B. Hooper, I. Cekic-Laskovic, A. Heuer, D. Bedrov, M. Winter, and G. Brunklaus, "Understanding transport mechanisms in ionic liquid/carbonate solvent electrolyte blends," Phys. Chem. Chem. Phys. 20, 16579 (2018).
- ¹⁸J. B. Haskins, W. R. Bennett, J. J. Wu, D. M. Hernández, O. Borodin, J. D. Monk, C. W. Bauschlicher, Jr., and J. W. Lawson, "Computational and experimental investigation of Li-doped ionic liquid electrolytes: [pyr14][TFSI], [pyr13][FSI], and [EMIM][BF₄]," J. Phys. Chem. B **118**, 11295–11309 (2014).
- ¹⁹V. Lesch, S. Jeremias, A. Moretti, S. Passerini, A. Heuer, and O. Borodin, "A combined theoretical and experimental study of the influence of different anion ratios on lithium ion dynamics in ionic liquids," J. Phys. Chem. B 118, 7367–7375 (2014).
- ²⁰N. Molinari, J. P. Mailoa, and B. Kozinsky, "Effect of salt concentration on ion clustering and transport in polymer solid electrolytes: A molecular dynamics study of PEO-LiTFSI," Chem. Mater. 30, 6298-6306 (2018).
- ²¹N. Molinari, J. P. Mailoa, and B. Kozinsky, "General trend of a negative Li effective charge in ionic liquid electrolytes," J. Phys. Chem. Lett. **10**, 2313–2319 (2019)
- ²²A. Wettstein, D. Diddens, and A. Heuer, "Controlling Li⁺ transport in ionic liquid electrolytes through salt content and anion asymmetry: A mechanistic understanding gained from molecular dynamics simulations," Phys. Chem. Chem. Phys. 24, 6072–6086 (2022).
- ²³W. Zhao, F. Leroy, B. Heggen, S. Zahn, B. Kirchner, S. Balasubramanian, and F. Müller-Plathe, "Are there stable ion-pairs in room-temperature ionic liquids? Molecular dynamics simulations of 1-*n*-butyl-3-methylimidazolium hexafluorophosphate," J. Am. Chem. Soc. **131**, 15825–15833 (2009).
- ²⁴B. R. Sundheim, "Transference numbers in molten salts," J. Phys. Chem. 60, 1381–1383 (1956).
- ²⁵B. R. Sundheim, "Transference phenomena in liquid electrolytes," J. Chem. Phys. 40, 27–32 (1964).
- ²⁶H. K. Kashyap, H. V. R. Annapureddy, F. O. Raineri, and C. J. Margulis, "How is charge transport different in ionic liquids and electrolyte solutions?," J. Phys. Chem. B 115, 13212–13221 (2011).

- ²⁷D. Dong, F. Sälzer, B. Roling, and D. Bedrov, "How efficient is Li⁺ ion transport in solvate ionic liquids under anion-blocking conditions in a battery?," Phys. Chem. Chem. Phys. **20**, 29174–29183 (2018).
- ²⁸K.-M. Tu, R. Ishizuka, and N. Matubayasi, "Spatial-decomposition analysis of electrical conductivity in ionic liquid," J. Chem. Phys. **141**, 244507 (2014).
- ²⁹K.-M. Tu, R. Ishizuka, and N. Matubayasi, "Spatial-decomposition analysis of electrical conductivity in concentrated electrolyte solution," J. Chem. Phys. **141**, 044126 (2014).
- ³⁰N. Matubayasi, "Spatial-decomposition analysis of electrical conductivity," Chem. Rec. 19, 723–734 (2019).
- ³¹ C. W. J. Beenakker, "Ewald sum of the Rotne-Prager tensor," J. Chem. Phys. 85, 1581-1582 (1986).
- ³²B. Dünweg, "Molecular dynamics algorithms and hydrodynamic screening," J. Chem. Phys. **99**, 6977–6982 (1993).
- ³³B. Dünweg and K. Kremer, "Molecular dynamics simulation of a polymer chain in solution," J. Chem. Phys. **99**, 6983–6997 (1993).
- ³⁴I.-C. Yeh and G. Hummer, "System-size dependence of diffusion coefficients and viscosities from molecular dynamics simulations with periodic boundary conditions," J. Phys. Chem. B 108, 15873–15879 (2004).
- 35 S. Gabl, C. Schröder, and O. Steinhauser, "Computational studies of ionic liquids: Size does matter and time too," J. Chem. Phys. 137, 094501 (2012).
- ³⁶O. Borodin, "Polarizable force field development and molecular dynamics simulations of ionic liquids," J. Phys. Chem. B **113**, 11463–11478 (2009).
- ³⁷D. Bedrov, J.-P. Piquemal, O. Borodin, A. D. MacKerell, Jr., B. Roux, and C. Schröder, "Molecular dynamics simulations of ionic liquids and electrolytes using polarizable force fields," Chem. Rev. 119, 7940–7995 (2019).
 ³⁸G. J. Martyna, M. L. Klein, and M. Tuckerman, "Nosé–Hoover chains: The
- ³⁸G. J. Martyna, M. L. Klein, and M. Tuckerman, "Nosé-Hoover chains: The canonical ensemble via continuous dynamics," J. Chem. Phys. **97**, 2635–2643 (1992).
- ³⁹ J.-P. Ryckaert, G. Ciccotti, and H. J. C. Berendsen, "Numerical integration of the cartesian equations of motion of a system with constraints: Molecular dynamics of *n*-alkanes," J. Comput. Phys. **23**, 327–341 (1977).
- ⁴⁰B. J. Palmer, "Direct application of SHAKE to the velocity Verlet algorithm," J. Comput. Phys. **104**, 470–472 (1993).
- ⁴¹G. J. Martyna, D. J. Tobias, and M. L. Klein, "Constant pressure molecular dynamics algorithms," J. Chem. Phys. **101**, 4177–4189 (1994).
- ⁴²G. J. Martyna, M. E. Tuckerman, D. J. Tobias, and M. L. Klein, "Explicit reversible integrators for extended systems dynamics," Mol. Phys. 87, 1117–1157 (1996).
- ⁴³S. von Bülow, J. T. Bullerjahn, and G. Hummer, "Systematic errors in diffusion coefficients from long-time molecular dynamics simulations at constant pressure," J. Chem. Phys. 153, 021101 (2020).
- ⁴⁴M. Kulke and J. V. Vermaas, "Reversible unwrapping algorithm for constant-pressure molecular dynamics simulations," J. Chem. Theory Comput. 18, 6161–6171 (2022).
- ⁴⁵J. N. A. Canongia Lopes and A. A. H. Pádua, "Nanostructural organization in ionic liquids," J. Phys. Chem. B 110, 3330–3335 (2006).
- ⁴⁶C. Hardacre, J. D. Holbrey, M. Nieuwenhuyzen, and T. G. A. Youngs, "Structure and solvation in ionic liquids," Acc. Chem. Res. 40, 1146–1155 (2007).
- ⁴⁷ M. Doi and S. F. Edwards, *The Theory of Polymer Dynamics* (Oxford University Press, 1988), Vol. 73.
- ⁴⁸R. M. Fuoss and L. Onsager, "The conductance of symmetrical electrolytes. III. Electrophoresis," J. Phys. Chem. **67**, 628–632 (1963).
- ⁴⁹W. H. Lee and R. J. Wheaton, "Conductance of symmetrical, unsymmetrical and mixed electrolytes. Part 2.—Hydrodynamic terms and complete conductance equation," J. Chem. Soc., Faraday Trans. 2 74, 1456–1482 (1978).
- ⁵⁰W. Ebeling, R. Feistel, and R. Sändig, "Electrolytic conductance for Gurney-Friedman models," J. Solution Chem. 8, 53–82 (1979).
- ⁵¹ A. R. Altenberger and H. L. Friedman, "Theory of conductance and related isothermal transport coefficients in electrolytes," J. Chem. Phys. **78**, 4162–4173 (1983).
- ⁵²B. L. Holian and D. J. Evans, "Shear viscosities away from the melting line: A comparison of equilibrium and nonequilibrium molecular dynamics," J. Chem. Phys. **78**, 5147–5150 (1983).

- ⁵³G. Hummer, L. R. Pratt, and A. E. García, "Molecular theories and simulation of ions and polar molecules in water," J. Phys. Chem. A 102, 7885–7895 (1998).
- ⁵⁴H. Hasimoto, "On the periodic fundamental solutions of the Stokes equations and their application to viscous flow past a cubic array of spheres," J. Fluid Mech. 5, 317–328 (1959).
- ⁵⁵T. Cao, X. Ji, J. Wu, S. Zhang, and X. Yang, "Correction of diffusion calculations when using two types of non-rectangular simulation boxes in molecular simulations," J. Mol. Model. 25, 22 (2019).
- ⁵⁶J. Mittal and G. Hummer, "Pair diffusion, hydrodynamic interactions, and available volume in dense fluids," J. Chem. Phys. **137**, 034110 (2012).
- ⁵⁷G. Hummer, "Position-dependent diffusion coefficients and free energies from Bayesian analysis of equilibrium and replica molecular dynamics simulations," New J. Phys. 7, 34 (2005).
- 58 J. Rotne and S. Prager, "Variational treatment of hydrodynamic interaction in polymers," J. Chem. Phys. 50 , $^{4831-4837}$ (1969).
- ⁵⁹F. Müller-Plathe, "Permeation of polymers—A computational approach," Acta Polym. 45, 259–293 (1994).
- ⁶⁰ A. Maitra and A. Heuer, "Understanding correlation effects for ion conduction in polymer electrolytes," J. Phys. Chem. B 112, 9641–9651 (2008).
- ⁶¹J. Farago, H. Meyer, and A. N. Semenov, "Anomalous diffusion of a polymer chain in an unentangled melt," Phys. Rev. Lett. 107, 178301 (2011).
- 62 J. Self, K. D. Fong, and K. A. Persson, "Transport in superconcentrated LiPF₆ and LiBF₄/propylene carbonate electrolytes," ACS Energy Lett. 4, 2843–2849 (2019).
- ⁶³R. Andersson, O. Borodin, and P. Johansson, "Dynamic structure discovery applied to the ion transport in the ubiquitous lithium-ion battery electrolyte LP30," J. Electrochem. Soc. 169, 100540 (2022).
- ⁶⁴T. Yamaguchi, T. Matsuoka, and S. Koda, "A theoretical study on the frequency-dependent electric conductivity of electrolyte solutions. II. Effect of hydrodynamic interaction," J. Chem. Phys. **130**, 094506 (2009).
- ⁶⁵ F. Figueirido, G. S. Del Buono, and R. M. Levy, "On finite-size effects in computer simulations using the Ewald potential," J. Chem. Phys. **103**, 6133–6142 (1995).
- ⁶⁶A. Kaintz, G. Baker, A. Benesi, and M. Maroncelli, "Solute diffusion in ionic liquids, NMR measurements and comparisons to conventional solvents," J. Phys. Chem. B **117**, 11697–11708 (2013).
- ⁶⁷O. Borodin and G. D. Smith, "LiTFSI structure and transport in ethylene carbonate from molecular dynamics simulations," J. Phys. Chem. B 110, 4971–4977 (2006).
- ⁶⁸B. K. Wheatle, N. A. Lynd, and V. Ganesan, "Effect of polymer polarity on ion transport: A competition between ion aggregation and polymer segmental dynamics," ACS Macro Lett. 7, 1149–1154 (2018).
- ⁶⁹ A. France-Lanord and J. C. Grossman, "Correlations from ion pairing and the Nernst-Einstein equation," Phys. Rev. Lett. 122, 136001 (2019).
- ⁷⁰P. Walden, "Über organische Lösungs-und Ionisierungsmittel," Z. Phys. Chem. 54U, 129–230 (1906).
- 71 M. Yoshizawa, W. Xu, and C. A. Angell, "Ionic liquids by proton transfer: Vapor pressure, conductivity, and the relevance of Δ pKa from aqueous solutions," J. Am. Chem. Soc. **125**, 15411–15419 (2003).
- ⁷² K. Ueno, H. Tokuda, and M. Watanabe, "Ionicity in ionic liquids: Correlation with ionic structure and physicochemical properties," Phys. Chem. Chem. Phys. 12, 1649–1658 (2010).
- ⁷³Y. Shao, K. Shigenobu, M. Watanabe, and C. Zhang, "Role of viscosity in deviations from the Nernst-Einstein relation," J. Phys. Chem. B **124**, 4774–4780 (2020).
- ⁷⁴T. Yamaguchi, "Coupling between the mesoscopic dynamics and shear stress of a room-temperature ionic liquid," Phys. Chem. Chem. Phys. 20, 17809–17817 (2018).
- ⁷⁵W. D. Amith, J. C. Araque, and C. J. Margulis, "Relationship between the relaxation of ionic liquid structural motifs and that of the shear viscosity," J. Phys. Chem. B **125**, 6264–6271 (2021).
- ⁷⁶E. Wacholder and D. Weihs, "Slow motion of a fluid sphere in the vicinity of another sphere or a plane boundary," Chem. Eng. Sci. 27, 1817–1828 (1972).

- ⁷⁷P. G. Wolynes and J. M. Deutch, "Slip boundary conditions and the hydrodynamic effect on diffusion controlled reactions," J. Chem. Phys. 65, 450–454 (1976).
- ⁷⁸Y. Yamada, J. Wang, S. Ko, E. Watanabe, and A. Yamada, "Advances and issues in developing salt-concentrated battery electrolytes," Nat. Energy **4**, 269–280 (2019).
- O. Borodin, J. Self, K. A. Persson, C. Wang, and K. Xu, "Uncharted waters: Super-concentrated electrolytes," Joule 4, 69–100 (2020).
 P. Simonnin, B. Noetinger, C. Nieto-Draghi, V. Marry, and B. Rotenberg,
- ⁸⁰P. Simonnin, B. Noetinger, C. Nieto-Draghi, V. Marry, and B. Rotenberg, "Diffusion under confinement: Hydrodynamic finite-size effects in simulation," J. Chem. Theory Comput. 13, 2881–2889 (2017).
- ⁸¹ M. Lorenz, F. Kilchert, P. Nürnberg, M. Schammer, A. Latz, B. Horstmann, and M. Schönhoff, "Local volume conservation in concentrated electrolytes is governing charge transport in electric fields," J. Phys. Chem. Lett. 13(37), 8751–8767 (1976).
 ⁸² S. H. Jamali, L. Wolff, T. M. Becker, A. Bardow, T. J. H. Vlugt, and O. A. Moul-
- ⁸²S. H. Jamali, L. Wolff, T. M. Becker, A. Bardow, T. J. H. Vlugt, and O. A. Moultos, "Finite-size effects of binary mutual diffusion coefficients from molecular dynamics," J. Chem. Theory Comput. 14, 2667–2677 (2018).
- ⁸⁵ A. T. Celebi, S. H. Jamali, A. Bardow, T. J. H. Vlugt, and O. A. Moultos, "Finite-size effects of diffusion coefficients computed from molecular dynamics: A review of what we have learned so far," Mol. Simul. 47, 831–845 (2021).